

A compressible viscous three-phase model for porous media flow based on the theory of mixtures

Yangyang Qiao*, Steinar Evje

University of Stavanger, Stavanger 4036, Norway

ARTICLE INFO

Keywords:

Multiphase flow in porous media
Three-phase flow
Viscous coupling
Mixture theory
Compressible model
Water alternating gas (WAG)
Waterflooding

ABSTRACT

In this paper we focus on a general model to describe compressible and immiscible three-phase flow in porous media. The underlying idea is to replace Darcy's law by more general momentum balance equations. In particular, we want to account for viscous coupling effects by introducing fluid-fluid interaction terms. In [Qiao, et al. (2018) Adv Water Resour 112: 170–188] a water-oil model based on the theory of mixtures was explored. It was demonstrated how the inclusion of viscous coupling effects could allow the model to better capture flow regimes which involve a combination of co-current and counter-current flow. In this work we extend the model in different aspects: (i) account for three phases (water, oil, gas) instead of two; (ii) deal with both the compressible and incompressible case; (iii) include viscous terms that represent frictional forces within the fluid (Brinkman type). A main objective of this work is to explore this three-phase model, which appears to be more realistic than standard formulation, in the context of petroleum related applications. We first provide development of stable numerical schemes in a one-dimensional setting which can be used to explore the generalized water-oil-gas model, both for the compressible and incompressible case. Then, several numerical examples with waterflooding in a gas reservoir and water alternating gas (WAG) experiments in an oil reservoir are investigated. Differences and similarities between the compressible and incompressible model are highlighted, and the fluid-fluid interaction effect is illustrated by comparison of results from the generalized model and a conventional model formulation.

1. Introduction

Generally

The processes of multiphase flow in porous media occur in many subsurface systems and have found many applications of practical interest, such as hydrology, petroleum engineering, geothermal energy development and carbon storage (Bakhshian et al., 2019; Bakhshian and Hosseini, 2019; Wu, 2016). The immiscible three-phase flow is always encountered in waterflooding for oil reservoirs with gas cap, in immiscible CO₂ storage in depleted oil and gas reservoirs, and steam floods and water-alternating-gas (WAG) processes (Bentsen and Trivedi, 2012; Juanes, 2008). Darcy's law was originally developed for single-phase flow (Darcy, 1856). Conventional modeling of multiphase flow is normally based on Darcy's extended law (Rose, 2000) by incorporation of relative permeabilities (Muskat et al., 1937). However, recent experimental observations indicate that the flow mode (co-current or counter-current) can have a strong impact on the flowing phase mobilities. That is to say, the relative permeabilities are not only function of saturation but are also related to the effect of how the fluids flow relatively to each other (Bentsen and Manai, 1992; Bourbiaux and Kalaydjian, 1990).

Viscous coupling

Viscous coupling (i.e., fluid-fluid interaction) was firstly mentioned by Yuster (1951) by using theoretical analysis to derive that relative permeability is a function of both saturation and viscosity ratio. In addition, capillary number was also proposed to be a factor affecting relative permeabilities (Ehrlich, 1993; Avraam and Payatakes, 1995). In general, momentum transfer due to differences in interstitial velocities induces acceleration of the slower and deceleration of the faster moving fluid when the fluids are moving co-currently. Deceleration of both fluid velocities will occur if they are moving counter-currently (Ayodele, 2006; Bentsen and Manai, 1993; Dullien and Dong, 1996; Li et al., 2004).

In order to extend the single-phase Darcy's law to multiphase flow, de la Cruz and Spanos (1983) derived theoretically Darcy's empirical extended law by applying the method of volume averaging to Stokes equation. In Kalaydjian (1987, 1990), Kalaydjian developed flow equations using the concepts of irreversible thermodynamics (Katchalsky and Curran, 1975) from a macroscopic understanding of two-phase flow in porous media. In addition, some researchers tried to gain insight into how two immiscible phases flow through a porous medium by using simple analogous models such as tubular flow (Yuster, 1951; Bacri et al., 1990). In Langaas and Papatzacos (2001) Langaas and Pa-

* Corresponding author.

E-mail address: steinar.evje@uis.no (Y. Qiao).

patzacos used the Lattice Boltzmann (LB) approach to investigate effects of viscous coupling and concluded that counter-current relative permeabilities caused partly by viscous coupling are always less than the corresponding co-current curves under different levels of capillary forces. Using the same method, Li et al. (2005) showed that their model was able to capture main experimental effects caused by viscous coupling. They also mentioned that the interfacial area between the fluids is a key variable for relative permeability functions for two immiscible fluids flow in porous media. A generalized model was developed in Qiao et al. (2018) for two-phase flow with viscous coupling effect. Numerical investigations showed a better agreement with the experimental tests (Bourbiaux and Kalaydjian, 1990) compared to the conventional modeling. The authors in Bentsen and Trivedi (2012) constructed modified transport equations for both co-current and counter-current three-phase flow through a vertical incompressible model based on partition concepts. Their equations are used to estimate the amount of model error because of a failure to account for the effect of interfacial coupling which has two types: viscous coupling and capillary coupling. Moreover, Sherafati and Jessen (2017) investigated the effect of mobility changes due to flow reversals from co-current to counter-current flow on the displacement of WAG injection processes.

Complex multiphase flow in porous media and use of the theory of mixtures

Motivated by petroleum related applications various attempts to solve the three-phase porous media flow model have been reported during the past decade (Falls and Schulte, 1992; Guzmán and Fayers, 1997a; 1997b; Juanes and Patzek, 2004). An interesting investigation was carried out in Lie and Juanes (2005) where a front-tracking algorithm was proposed for constructing very accurate solutions to one-dimensional problems (for example WAG test therein). This was explored in the context of streamline simulation which decouples the three-dimensional problem into a set of one-dimensional problems along streamlines. This work is limited to three-phase immiscible, incompressible flow and also gravity and capillarity were ignored. Different numerical methods have been implemented to simulate three-phase flow in porous media. A finite volume method was used in Lee et al. (2008) for solving compressible, immiscible flow with gravity in heterogeneous formations by using the black oil formulation. A hybrid-upwinding scheme for phase flux was proposed in Lee and Efendiev (2016) for a finite difference approximation to solve the three phase transport equations in the presence of viscous and buoyancy forces. A finite element method was applied to simulate fluid injection and imbibition processes in a deformable porous media (Gajo et al., 2017). Moreover, (Dong and Rivière, 2016) applied a semi-implicit method with discontinuous Galerkin (DG) discretization to solve the incompressible three-phase flow in two dimensions. Additional physical effects are also discussed and explored for three-phase porous media flow, such as hysteresis effects of relative permeabilities (Ranaee et al., 2019) and elliptic regions (Juanes and Patzek, 2004; Juanes, 2008; Lee and Efendiev, 2016). In Juanes (2008) Juanes presented a nonequilibrium model of incompressible three-phase flow in porous media. The nonequilibrium effects by introducing a pair of effective water and gas saturations into the formulations have the ability to smear saturation fronts from numerical simulations.

The theory of mixtures offers a general framework for developing models for complex multiphase flow systems (Rajagopal, 2007). More lately, biomedical applications have been a driver for the development of various models relying on this approach. For example, the study how cancer cells are able to break loose from a primary tumor involves a solid matrix (the so-called extracellular matrix), different type of cells (cancer cells, stromal cells, immune cells), and interstitial fluid (Evje, 2017; Evje and Waldeland, 2019). A recent example of this is described in Waldeland and Evje (2018b); Urdal et al. (2019) where, respectively, a cell-fluid two-phase model and a cell-fibroblast-fluid three-phase model are developed to shed light on the experimentally observed tumor cell behavior reported in Shieh et al. (2011). The model that is derived

relies on replacing Darcy's law by more general momentum balance equations which incorporate both the cell-matrix resistance force and the cell-fibroblast interaction. The latter is understood as a "viscous coupling" effect caused by a mechanical coupling that can occur between tumor cells and fibroblasts and has been reported in experimental studies (Labernadie, 2017). Another example how generalized momentum equations can be used to capture non-standard multiphase behavior in the context of aggressive tumor cells is explored in Waldeland and Evje (2018a). In Polacheck et al. (2011) two competing migration mechanisms were observed, one in the upstream direction and another in the downstream direction. The use of generalized momentum equations allowed us to account for both this fluid-stress generated upstream migration and a chemotactic migration in the direction of increasing concentration of chemical concentrations (Waldeland and Evje, 2018a).

The aim of this work

The objective of this paper is to investigate a mixture theory approach to simulate three immiscible fluids flowing in a 1D reservoir. We shall consider both the case with compressible and incompressible fluids. The model which is introduced is quite general since it can automatically capture flow that involves a combination of co-current and counter-current flow. The current work represents extension of previous work in two ways:

- Extend the incompressible two-phase model that was explored in Qiao et al. (2018); Andersen et al. (2019) to include three phases.
- Extend the compressible two-phase model studied in Qiao et al. (2019a) to include three phases.

In addition, the models we study in the current work are more general than those studied in Qiao et al. (2018); Andersen et al. (2019) since we consider Stokes like momentum equations which involve viscous terms that account for internal friction due to viscosity. In particular, appropriate numerical schemes are introduced to investigate compressible and incompressible three-phase flow scenarios that are motivated by injection-production flow scenarios.

Main observations from our numerical experiments with two and three-phase flow scenarios where the flow dynamics are generated by injection of water or gas in the center of the domain and production of fluids at the left and right boundary are: (i) The simulation cases involve competition between pressure driven co-current flow and counter-current gravity driven flow; (ii) Both the incompressible and compressible discrete version of the model appear to have good stability properties. The numerical experiments indicate that the numerical schemes can be useful as a tool to deepen the insight into the relation between the incompressible and compressible version of the model. The model and its discrete approximate counterparts appear to be a good starting point for extending to more complex flow systems, as mentioned above, that involve competition between different distinct, non-standard transport mechanisms.

The rest of this paper is organized as follows. In Section 2 we briefly describe the mixture flux approach in a three-phase setting. In Section 3 we summarize the generalized three-phase porous media model, both a compressible and an incompressible version of it. Section 4 is devoted to numerical simulations to demonstrate three-phase dynamics and verify basic features of the numerical schemes. The details of the compressible and incompressible scheme are given in Appendix A–Appendix D.

2. Mixture theory framework

2.1. Conventional model based on Darcy's law

We firstly describe the traditional formulation of incompressible multiphase flow model without source terms. Transport equations for

incompressible and immiscible phases oil (*o*), water (*w*) and gas (*g*) in porous media are normally given by:

$$\partial_t(\phi s_i) + \nabla \cdot \mathbf{U}_i = Q_i, \tag{2.1}$$

$$\mathbf{U}_i = \phi s_i \mathbf{u}_i, \quad (i = w, o, g), \tag{2.2}$$

where ϕ is porosity, s_i is phase saturation, Q_i is the source term, and \mathbf{U}_i and \mathbf{u}_i are the Darcy velocity and interstitial velocity of each phase $i = o, w, g$, respectively. For simplicity the irreducible (immobile) phase saturation (s_{ir}) is not considered in the equations by assuming it is equal to 0. Hence, the normalized phase saturation ($= \frac{s_i - s_{ir}}{1 - s_{wr} - s_{or} - s_{gr}}$) equals the phase saturation value s_i . The traditional macroscopic formulation of Darcy's law that relates the volumetric flux of a phase to the pressure gradient of that phase is given by:

$$\mathbf{U}_i = -\frac{K k_{ri}}{\mu_i} (\nabla p_i - \rho_i \mathbf{g}), \quad (i = w, o, g), \tag{2.3}$$

where K is the absolute permeability of porous media, p_i is phase pressure, \mathbf{g} is the acceleration of gravity and k_{ri} , ρ_i and μ_i are phase relative permeability, density and viscosity, respectively.

2.2. A generalized multiphase flow model based on mixture theory

For our investigations, the mass balance equations with source terms in the case of compressible water-oil-gas transport can be given by:

$$\begin{aligned} (\phi n_w)_t + \nabla \cdot (\phi n_w u_w) &= -n_w Q_p + \rho_w Q_{Iw}, & n_w &= s_w \rho_w \\ (\phi n_o)_t + \nabla \cdot (\phi n_o u_o) &= -n_o Q_p, & n_o &= s_o \rho_o \\ (\phi n_g)_t + \nabla \cdot (\phi n_g u_g) &= -n_g Q_p + \rho_g Q_{Ig}, & n_g &= s_g \rho_g \end{aligned} \tag{2.4}$$

where u_i , ($i = w, o, g$) represents the interstitial velocity of phase i in the porous media. In addition, Q_p is the production rate and Q_{Iw} , Q_{Ig} represent the injection rate of water and gas, respectively.

The starting point for developing our model that can account for more detailed physical mechanisms for water-oil-gas porous media flow than conventional modeling, is the theory of mixtures. This is a theory based on balance laws and conservation principles, which is well known in continuum mechanics (Bowen, 1976; Rajagopal and Tao, 1995; Byrne and Preziosi, 2003; Ambrosi and Preziosi, 2002; Preziosi and Farina, 2002), and has been widely applied to the biological tumor-growth systems which can be characterized as a mixture of interacting continua.

Neglecting inertial effects (acceleration effects), as is usual when dealing with creeping flow in porous materials, the mechanical stress balance is given by Ambrosi and Preziosi (2002):

$$0 = \nabla \cdot (s_i \sigma_i) + m_i + G_i, \quad (i = w, o, g), \tag{2.5}$$

where σ_i refers to the Cauchy stress tensor, m_i represents the interaction forces exerted on the constituents by other constituents of the mixture, and $G_i = s_i \rho_i \mathbf{g}$ is the external body force due to gravity. The standard expression for the stress terms σ_i , is given by

$$\sigma_i = -p_i \delta + \tau_i, \quad (i = w, o, g), \tag{2.6}$$

where δ is the unitary tensor and

$$\tau_i = 2\mu_i e_i, \quad e_i = \frac{1}{2}(\nabla u_i + \nabla u_i^T), \quad (i = w, o, g). \tag{2.7}$$

The viscous part τ_i reflects that the water, oil and gas behave as a viscous fluid. According to general principles of the theory of mixtures, the interaction forces m_i between the constituents appearing in (2.5) may be described as in Preziosi and Farina (2002); Ambrosi and Preziosi (2002); Byrne and Preziosi (2003):

$$\begin{aligned} m_o &= p_o \nabla s_o + F_{wo} - F_{og} + M_{om}, \\ m_w &= p_w \nabla s_w - F_{wo} - F_{wg} + M_{wm}, \\ m_g &= p_g \nabla s_g + F_{wg} + F_{og} + M_{gm}, \end{aligned} \tag{2.8}$$

where F_{ij} ($i, j = o, w, g$), denotes the force (drag) that the i phase exerts on the j phase. The j phase exerts an equal and opposite force $-F_{ij}$. Similarly, M_{om} , M_{wm} and M_{gm} represent interaction forces (drag forces) between fluid and pore walls (solid matrix), respectively, for oil, water and gas. The term $p_i \nabla s_i$ is related to interfacial force exerted by other phases on phase i , arising from mathematical derivation of averaged equations (Drew and Segel, 1971). To close the system we must specify the drag force term F_{wo} , F_{wg} , and F_{og} and the stresses σ_i ($i = o, w, g$) and interaction force terms M_{im} between fluid ($i = w, o, g$) and matrix. Drag force represents the interaction between one phase and another phase and is modelled as Rajagopal (2007); Preziosi and Farina (2002); Ambrosi and Preziosi (2002):

$$\begin{aligned} F_{wo} &= \hat{k}_{wo}(u_w - u_o), \\ F_{wg} &= \hat{k}_{wg}(u_w - u_g), \\ F_{og} &= \hat{k}_{og}(u_o - u_g), \end{aligned} \tag{2.9}$$

where \hat{k}_{ij} ($i, j = o, w, g$), remains to be determined. Typically, $\hat{k}_{ij} \sim s_i s_j$ to reflect that this force term will vanish when one of the phases vanishes. Similarly, the interaction force between fluid and pore wall (matrix, which is stagnant) is naturally expressed then as (Rajagopal and Tao, 1995; Rajagopal, 2007; Preziosi and Farina, 2002; Ambrosi and Preziosi, 2002):

$$M_{im} = -\hat{k}_i u_i, \quad (i = o, w, g). \tag{2.10}$$

The coefficients \hat{k}_{ij} and \hat{k}_i (dimension $\text{Pa} \cdot \text{s}/\text{m}^2$), that characterize the magnitude of interaction terms, can be chosen such that the model recovers the classical porous media model based on Darcy's law. At the same time the approach used here will open for development of reservoir models where more detailed physics can be taken into account.

3. A summary of the general three-fluid model for porous media flow

3.1. The compressible case

We are interested in studying a 1-D model for three compressible immiscible fluids moving in a porous media. After combining (2.4)-(2.10) the model takes the following form:

$$\begin{aligned} (\phi n_w)_t + (\phi n_w u_w)_x &= -n_w Q_p + \rho_w Q_{Iw}, & n_w &= s_w \rho_w, \\ (\phi n_o)_t + (\phi n_o u_o)_x &= -n_o Q_p, & n_o &= s_o \rho_o, \\ (\phi n_g)_t + (\phi n_g u_g)_x &= -n_g Q_p + \rho_g Q_{Ig}, & n_g &= s_g \rho_g \\ s_w(P_w)_x &= -\hat{k}_w u_w - \hat{k}_{wo}(u_w - u_o) - \hat{k}_{wg}(u_w - u_g) \\ &\quad + n_w g + \varepsilon_w (n_w u_{wx})_x, \\ s_o(P_o)_x &= -\hat{k}_o u_o - \hat{k}_{wo}(u_o - u_w) - \hat{k}_{og}(u_o - u_g) \\ &\quad + n_o g + \varepsilon_o (n_o u_{ox})_x, \\ s_g(P_g)_x &= -\hat{k}_g u_g - \hat{k}_{wg}(u_g - u_w) - \hat{k}_{og}(u_g - u_o) \\ &\quad + n_g g + \varepsilon_g (n_g u_{gx})_x, \\ \Delta P_{ow}(s_w) &= P_o - P_w, & \Delta P_{go}(s_g) &= P_g - P_o \end{aligned} \tag{3.11}$$

with capillary pressure ΔP_{ow} defined as the pressure difference between the oil and water and capillary pressure ΔP_{go} defined as the pressure difference between the gas and oil. We may choose to use the following expressions for capillary force

$$\begin{aligned} \Delta P_{ow} &= P_o - P_w = \Delta P_{ow}(s_w) = -P_{c1}^* \ln(\delta_1 + \frac{s_w}{a_1}) \quad \text{and} \quad \delta_1, a_1 > 0, \\ \Delta P_{go} &= P_g - P_o = \Delta P_{go}(s_g) = P_{c2}^* s_g^{a_2} \quad \text{and} \quad a_2 > 0 \end{aligned} \tag{3.12}$$

with non-negative constants P_{ci}^* representing interfacial tension. This allows us to mimic capillary pressure functions that previously have been proposed for three-phase reservoir flow (Chen and Ewing, 1997;

Odd and David, 2010). In addition, we have the fundamental relation that the three phases fill the pore space

$$s_o + s_w + s_g = 1. \quad (3.13)$$

The above model must be combined with appropriate closure relations for $\rho_i = \rho_i(P_i)$. We represent the three phases by linear pressure-density relations of the form

$$\rho_w - \bar{\rho}_{w0} = \frac{P_w}{C_w}, \quad \rho_o - \bar{\rho}_{o0} = \frac{P_o}{C_o}, \quad \rho_g = \frac{P_g}{C_g} \quad (3.14)$$

where C_w , C_o and C_g represent the inverse of the compressibility of water, oil and gas, respectively.

We refer to Appendix B for a semi-discrete approximation of (3.11) as well as a fully discrete scheme.

Remark 3.1. We may also study a higher dimensional case (e.g., 2D) where the model consists of three mass balance equations for three phases (water, oil and gas) and six momentum equations (each phase has two directions such as x and y). The scheme has been tested in 2D for two phases and shows similar properties as in 1D.

3.2. The incompressible case

3.2.1. Viscous flow

We may let C_w, C_o, C_g go to infinity in (3.14). Then we obtain the incompressible version of the model (3.11). We refer to Appendix C for a semi-discrete as well as a fully discrete scheme for this incompressible case.

3.2.2. Inviscid flow

Moreover, in order to relate this incompressible version to the classical Darcy-based formulation we ignore the viscosity terms in the momentum equations by setting $\varepsilon_i = 0 (i = w, o, g)$ in (3.11)_{4,5,6}. Solving momentum equations with respect to interstitial phase velocities u_i , the Darcy velocities of fluid phase are expressed as follows based on (2.2):

$$\begin{aligned} U_w &= \phi s_w u_w = -\lambda_{ww}(P_{wx} - \rho_w g) - \lambda_{wo}(P_{ox} - \rho_o g) - \lambda_{wg}(P_{gx} - \rho_g g), \\ U_o &= \phi s_o u_o = -\lambda_{wo}(P_{wx} - \rho_w g) - \lambda_{oo}(P_{ox} - \rho_o g) - \lambda_{og}(P_{gx} - \rho_g g), \\ U_g &= \phi s_g u_g = -\lambda_{wg}(P_{wx} - \rho_w g) - \lambda_{og}(P_{ox} - \rho_o g) - \lambda_{gg}(P_{gx} - \rho_g g), \end{aligned} \quad (3.15)$$

and the following relations are defined:

$$\begin{aligned} \lambda_{ww} &= \frac{\phi s_w^2}{R} (R_o R_g - \hat{k}_{og}^2), & \lambda_{wo} &= \lambda_{ow} = \frac{\phi s_w s_o}{R} (\hat{k}_{wo} R_g + \hat{k}_{og} \hat{k}_{wg}), \\ \lambda_{oo} &= \frac{\phi s_o^2}{R} (R_w R_g - \hat{k}_{wg}^2), & \lambda_{wg} &= \lambda_{gw} = \frac{\phi s_w s_g}{R} (\hat{k}_{wg} R_o + \hat{k}_{og} \hat{k}_{wo}), \\ \lambda_{gg} &= \frac{\phi s_g^2}{R} (R_w R_o - \hat{k}_{wo}^2), & \lambda_{go} &= \lambda_{og} = \frac{\phi s_o s_g}{R} (\hat{k}_{og} R_w + \hat{k}_{wg} \hat{k}_{wo}), \end{aligned} \quad (3.16)$$

where

$$\begin{aligned} R_w &= \hat{k}_w + \hat{k}_{wg} + \hat{k}_{wo}, \\ R_o &= \hat{k}_o + \hat{k}_{wo} + \hat{k}_{og}, \\ R_g &= \hat{k}_g + \hat{k}_{wg} + \hat{k}_{og}, \\ R &= \hat{k}_w \hat{k}_o \hat{k}_g + (\hat{k}_w + \hat{k}_o + \hat{k}_g)(\hat{k}_{wg} \hat{k}_{wo} + \hat{k}_{og} \hat{k}_{wo} + \hat{k}_{wg} \hat{k}_{og}) \\ &\quad + \hat{k}_g \hat{k}_w (\hat{k}_w + \hat{k}_o) + \hat{k}_w \hat{k}_{og} (\hat{k}_o + \hat{k}_g) + \hat{k}_o \hat{k}_{wg} (\hat{k}_w + \hat{k}_g). \end{aligned} \quad (3.17)$$

Using capillary pressure relations (3.12) it follows that (3.15) take the following equivalent form:

$$\begin{aligned} U_w &= -\hat{\lambda}_w P_{wx} - (\lambda_{wo} + \lambda_{wg}) \Delta P_{owx} - \lambda_{wg} \Delta P_{gox} \\ &\quad + (\lambda_{ww} \rho_w + \lambda_{wo} \rho_o + \lambda_{wg} \rho_g) g, \\ U_o &= -\hat{\lambda}_o P_{wx} - (\lambda_{oo} + \lambda_{og}) \Delta P_{owx} - \lambda_{og} \Delta P_{gox} + (\lambda_{wo} \rho_w + \lambda_{oo} \rho_o + \lambda_{og} \rho_g) g, \\ U_g &= -\hat{\lambda}_g P_{wx} - (\lambda_{gg} + \lambda_{og}) \Delta P_{owx} - \lambda_{gg} \Delta P_{gox} \\ &\quad + (\lambda_{wg} \rho_w + \lambda_{og} \rho_o + \lambda_{gg} \rho_g) g. \end{aligned} \quad (3.18)$$

Here we define the following notation for generalized phase mobilities $\hat{\lambda}_i$:

$$\begin{aligned} \hat{\lambda}_w &= \lambda_{ww} + \lambda_{wo} + \lambda_{wg}, \\ \hat{\lambda}_o &= \lambda_{oo} + \lambda_{wo} + \lambda_{og}, \\ \hat{\lambda}_g &= \lambda_{gg} + \lambda_{wg} + \lambda_{og}. \end{aligned} \quad (3.19)$$

By summing U_w, U_o and U_g in (3.18) and using the notation introduced in (3.19), the total Darcy velocity can be expressed as follows:

$$U_T = -\hat{\lambda}_T P_{wx} - (\hat{\lambda}_o + \hat{\lambda}_g) \Delta P_{owx} - \hat{\lambda}_g \Delta P_{gox} + (\hat{\lambda}_w \rho_w + \hat{\lambda}_o \rho_o + \hat{\lambda}_g \rho_g) g \quad (3.20)$$

where we have used

$$\hat{\lambda}_T = \hat{\lambda}_w + \hat{\lambda}_o + \hat{\lambda}_g. \quad (3.21)$$

Therefore, the water pressure gradient can be derived from (3.20):

$$P_{wx} = -\frac{1}{\hat{\lambda}_T} U_T - (\hat{f}_o + \hat{f}_g) \Delta P_{owx} - \hat{f}_g \Delta P_{gox} + (\hat{f}_w \rho_w + \hat{f}_o \rho_o + \hat{f}_g \rho_g) g \quad (3.22)$$

with generalized fractional flow function:

$$\hat{f}_i = \hat{\lambda}_i / \hat{\lambda}_T, \quad (i = w, o, g). \quad (3.23)$$

Inserting (3.22) into (3.18) we get:

$$\begin{aligned} U_w &= \hat{f}_w U_T + (W_o + W_g) \Delta P_{owx} + W_g \Delta P_{gox} - (W_w \rho_w + W_o \rho_o + W_g \rho_g) g, \\ U_o &= \hat{f}_o U_T + (O_o + O_g) \Delta P_{owx} + O_g \Delta P_{gox} - (O_w \rho_w + O_o \rho_o + O_g \rho_g) g, \\ U_g &= \hat{f}_g U_T + (G_o + G_g) \Delta P_{owx} + G_g \Delta P_{gox} - (G_w \rho_w + G_o \rho_o + G_g \rho_g) g, \end{aligned} \quad (3.24)$$

where

$$\begin{aligned} W_i &= \hat{\lambda}_w \hat{f}_i - \lambda_{wi}, \\ O_i &= \hat{\lambda}_o \hat{f}_i - \lambda_{oi}, \\ G_i &= \hat{\lambda}_g \hat{f}_i - \lambda_{gi}, \quad (i = w, o, g). \end{aligned} \quad (3.25)$$

It should be noted that $W_i + O_i + G_i = 0 (i = w, o, g)$ in light of (3.16), (3.21), and (3.23).

4. Numerical examples

We mainly focus on a reservoir model where there are one injection well at the center and two production wells distributed at two sides. The injection rate is equal to the total production rate and the rates of two production wells are also same (See Fig. 1). In addition, reservoir inclination θ is also accounted for in the model.

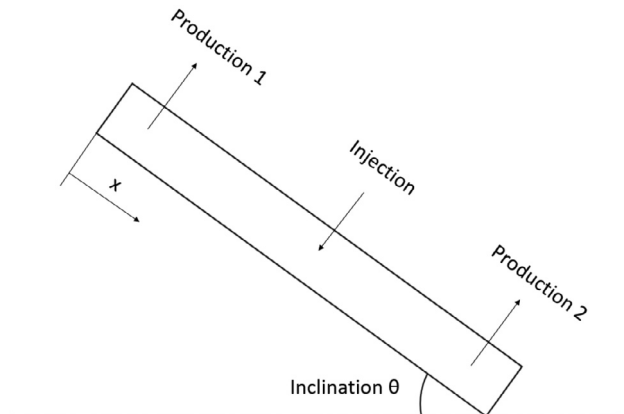


Fig. 1. Reservoir model with injection and production.

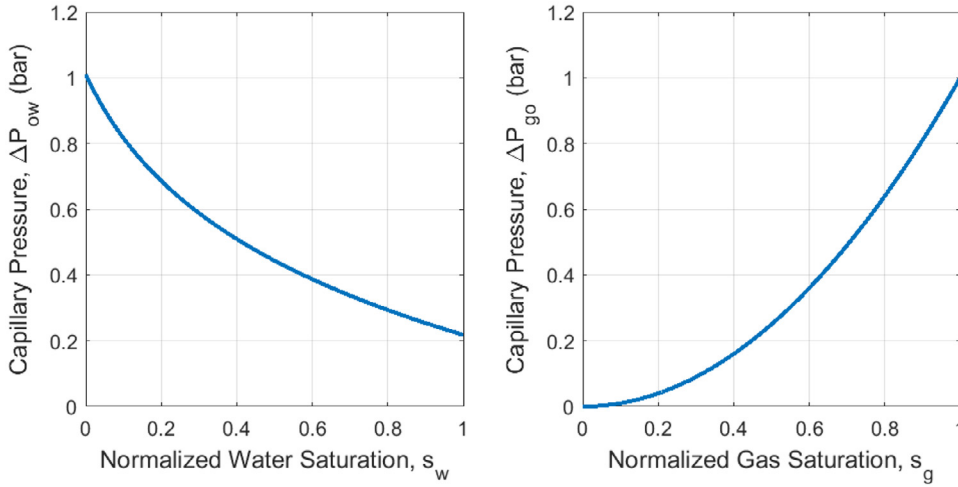


Fig. 2. Left: Capillary pressure between water and oil. Right: Capillary pressure between oil and gas. We refer to (3.12) for their expressions and Table 1 for the input parameters.

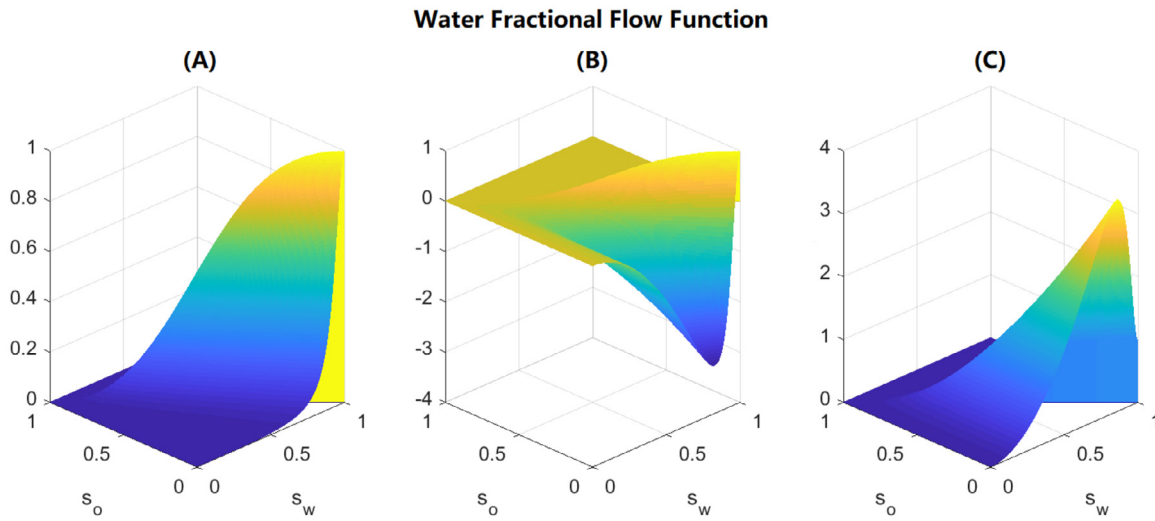


Fig. 3. Water fractional flow function $f_w(s_w, s_o)$ (defined in (4.27)) with effects of model inclination θ and total flow direction of U_T . (A): $\sin\theta = 0$, $U_T = \bar{Q}_p/2$; (B): $\sin\theta = 1$, $U_T = -\bar{Q}_p/2$; (C): $\sin\theta = 1$, $U_T = \bar{Q}_p/2$.

Interaction terms

The model (3.11)_{4,5,6} should be armed with appropriate functional correlations for fluid-rock resistance force $\hat{k}_w, \hat{k}_o, \hat{k}_g$ and fluid-fluid drag force $\hat{k}_{wo}, \hat{k}_{wg}, \hat{k}_{og}$. Here we use the interaction terms suggested in the recent works (Standnes et al., 2017; Qiao et al., 2018; Andersen et al., 2019):

$$\begin{aligned} \hat{k}_w &:= I_w s_w^\alpha \frac{\mu_w}{K} \phi, & \hat{k}_o &:= I_o s_o^\beta \frac{\mu_o}{K} \phi, & \hat{k}_g &:= I_g s_g^\gamma \frac{\mu_g}{K} \phi, \\ \hat{k}_{wo} &:= I_{wo} s_w s_o \frac{\mu_w \mu_o}{K} \phi, & \hat{k}_{wg} &:= I_{wg} s_w s_g \frac{\mu_w \mu_g}{K} \phi, & \hat{k}_{og} &:= I_{og} s_o s_g \frac{\mu_o \mu_g}{K} \phi. \end{aligned} \quad (4.26)$$

All the interaction terms \hat{k}_i and \hat{k}_{ij} have dimension $\text{Pa} \cdot \text{s}/\text{m}^2$. The parameters α, β and γ are dimensionless exponents whereas I_w, I_o and I_g are dimensionless friction coefficients characterizing the strength of fluid-solid interaction. Finally, I_{wo}, I_{wg} and I_{og} are coefficients characterizing the strength of the fluid-fluid drag force with dimension $(\text{Pa} \cdot \text{s})^{-1}$.

Input data

The input parameters used in the simulations are listed in Table 1. We use 101 grid cells for a 100-meter reservoir layer. We refer to Appendix D for a convergence test. The magnitude of the interaction coefficients I_{wo}, I_{wg} , and I_{og} are chosen as in Qiao et al. (2018) where we applied a generalized two-phase model to match the experimentally measured relative permeability curves and obtained values for the input parameters such as I_{wo} whose magnitude is around several thousands. In order to avoid too many complicating effects at the same time in the subsequent discussion, we have set the viscosity terms to zero, i.e., $\epsilon_w = \epsilon_o = \epsilon_g = 0$.

We use the similar capillary pressure relations as Qiao et al. (2019b) for water and oil and Lewis and Pao (2002) for oil and gas (see Fig. 2). The expression of an effective water fractional flow function $f_w(s_w, s_o)$ in the conventional water-oil-gas model (assuming no capillary pressure, i.e., $\Delta P_{ow} = \Delta P_{go} = 0$) is

$$f_w(s_w, s_o) \stackrel{\text{def}}{=} \frac{U_w}{U_T} = \frac{\frac{\lambda_w}{\lambda_T} U_T - (W_w \rho_w + W_o \rho_o + W_g \rho_g) g \sin \theta}{U_T} \quad (4.27)$$

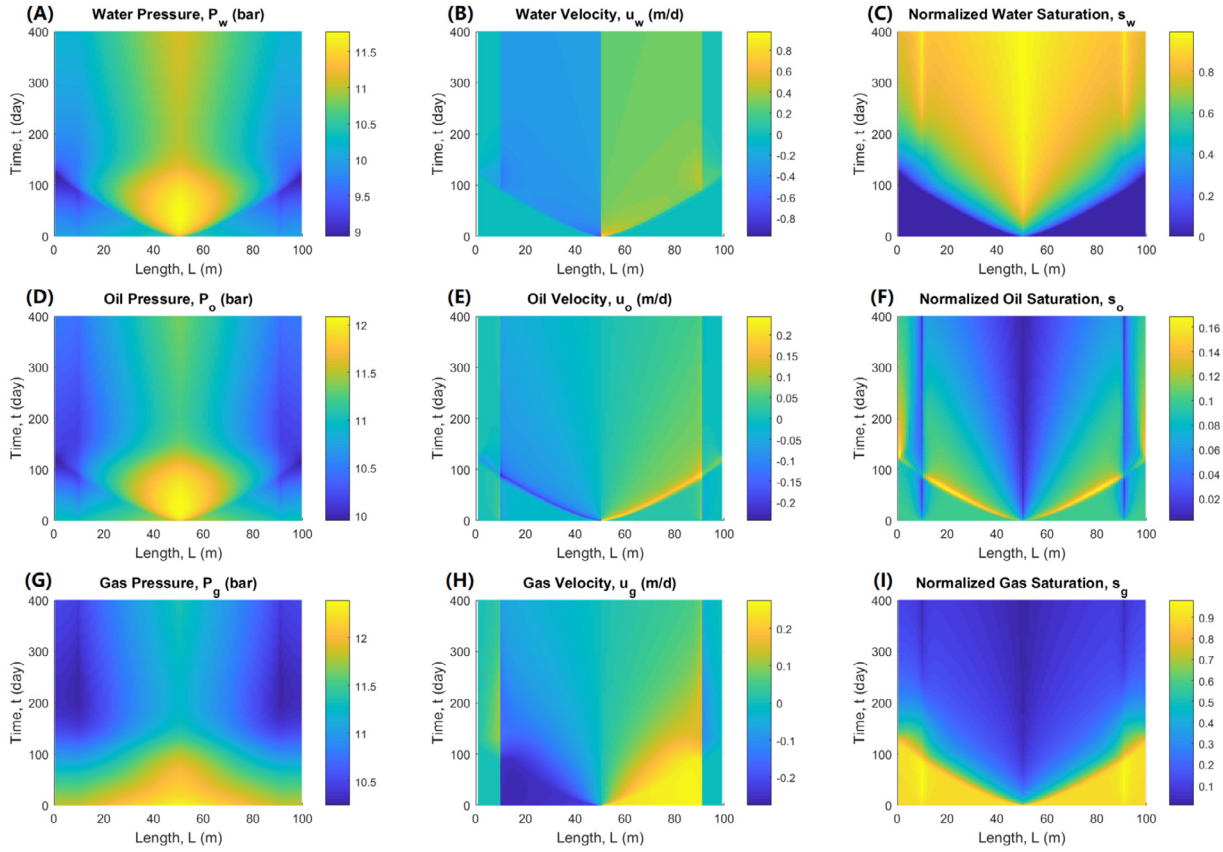


Fig. 4. Results of the horizontal compressible three-phase model during a 400-day waterflooding period. The source term effects can be seen clearly in all plots where production wells are located at 10 m and 90 m and injection well at 50 m. (A) Water pressure plot shows a strong pressure gradient region at the early stage (before 130 days). (B) Water velocity profile. It can be seen that water— front reaches the production well after around 100 days. (C) Normalized water saturation shows that the water front is fast whereas the other phases (oil and gas) are produced slowly (takes almost 300 days). (D) Oil pressure profile gives a similar result as water pressure. (E) Oil velocity behavior is similar to water velocity. (F) Normalized oil saturation plot illustrates that oil is displaced quite slowly. (G) The gas pressure gradient is very low in the gas-displaced region at the early stage due to the high mobility of gas. (H) There is no gas advancing front since gas flows easily. (I) Gas is displaced fastly and a lot of gas is recovered before 130 days.

Table 1
Reference input parameters in the simulations.

Parameter	Dimensional value	Parameter	Dimensional value
L	100 m	I_w	2.5
ϕ	0.25	I_o	1.8
$\bar{\rho}_{w0}$	1 g/cm ³	I_g	1.1
$\bar{\rho}_{o0}$	0.8 g/cm ³	I_{wo}	3000 (Pa · s) ⁻¹
$\bar{\rho}_{g0}$	0.018 g/cm ³	I_{wg}	3000 (Pa · s) ⁻¹
S_{wr}	0	I_{og}	3000 (Pa · s) ⁻¹
S_{or}	0	α	0.01
S_{gr}	0	β	0.01
μ_w	1 cP	γ	0.01
μ_o	1.5 cP	P_{c1}^*	4 · 10 ⁴ Pa
μ_g	0.015 cP	a_1	2
K	1000 mD	δ_1	0.08
k_{rw}^{max}	0.4	P_{c2}^*	10 ⁵ Pa
k_{ro}^{max}	0.5556	a_2	2
k_{rg}^{max}	0.9091	C_w	10 ⁶ m ² /s ²
\bar{Q}_{Iw}	0.125 m ³ /day	C_o	5 · 10 ⁵ m ² /s ²
\bar{Q}_{Ig}	0.125 m ³ /day	C_g	10 ⁵ m ² /s ²
\bar{Q}_p	0.0625 m ³ /day	ϵ_w	0.0 cP
N_x	101	ϵ_o	0.0 cP
A	1 m ²	ϵ_g	0.0 cP
P_{wL}	10 ⁶ Pa	x_I	50 m
Δt	1570 s	$x_{P(1,2)}$	10 ₍₁₎ &90 ₍₂₎ m

where we have used (3.24) and (3.25) where $U_T = \int_0^x (Q_I - Q_p) dx$. Similarly, f_o and f_g can also be expressed in the same manner. In order to illustrate the phase flow fraction f_w (see Fig. 3) we represent U_T by a

reference total velocity $\bar{U}_T \in [-\frac{\bar{Q}_p}{2}, +\frac{\bar{Q}_p}{2}]$. We refer to Table 1 for other input data that are used.

Initial conditions

For the waterflooding case, we assume the reservoir initially is mostly filled with gas (90%) and some oil (10%):

$$s_g(x, t = 0) = 0.9, \quad s_o(x, t = 0) = 0.1. \tag{4.28}$$

For the WAG injection case, the reservoir is assumed initially filled with oil (90%) and some extra water (10%):

$$s_o(x, t = 0) = 0.9, \quad s_w(x, t = 0) = 0.1. \tag{4.29}$$

For the compressible case, a reference pressure P_{wL} at the left boundary of the layer is given at initial state,

$$P_{wL}(x = 0, t = 0) = 10^6 \text{ Pa}. \tag{4.30}$$

Boundary conditions

We assume a closed boundary for both compressible and incompressible models, which means that

$$u_i(x = 0, t) = 0, \quad u_i(x = L, t) = 0, \quad i = w, o, g. \tag{4.31}$$

For the incompressible case, we give a reference pressure P_{wL} at the left boundary of the layer,

$$P_{wL}(x = 0, t) = 10^6 \text{ Pa}. \tag{4.32}$$

Source terms

For WAG experiments, gas and water are injected at different time periods during the whole oil recovery process. We assume that $Q_i(x)$ and $Q_p(x)$ take the form

$$Q_{I_w, I_g}(x) = \frac{\bar{Q}_{I_w, I_g}}{\sigma} \begin{cases} 1, & \text{if } |x - x_I| \leq \sigma/2; \\ 0, & \text{otherwise.} \end{cases},$$

$$Q_p(x) = \frac{\bar{Q}_p}{\sigma} \begin{cases} 1, & \text{if } |x - x_{p,i}| \leq \sigma/2; \\ 0, & \text{otherwise.} \end{cases} \quad (4.33)$$

where $(i = 1, 2)$ and $\bar{Q}_{I_w, I_g} = 0.125\text{m}^3/\text{day}$ and $\bar{Q}_p = 0.0625\text{m}^3/\text{day}$. The width of the small region associated with the injector and producer is σ . In the numerical scheme $\sigma = \Delta x$.

4.1. Waterflooding in a gas reservoir

We first test the proposed compressible three-phase model applied to a gas reservoir development. In this example, water is injected at 50 m into a gas reservoir layer of length 100 m with a little proportion of oil (10%). Two cases, respectively, for the horizontal (Fig. 4) and vertical reservoir (Fig. 5) are shown below.

The results of the horizontal compressible three-phase model with water injection for a total period of 400 days are shown in Fig. 4 where pressures (first column), velocities (middle column) and saturations (right column) are symmetric with the injection well located at the center of reservoir layer. The gas is mostly recovered during the first 130 days, see (I), whereas oil recovery takes place over more than 300 days, see (F), due to its lower mobility than gas. It is also observed that at early stage gas pressure along the reservoir layer has less gradient than both the water's and the oil's (see first column in Fig. 4). The injected water displaces both oil and gas in the reservoir near the injection well region where a high pressure gradient is necessary for both water and oil to flow, see panel (A) and (B), because of their low mobilities. After water has arrived the production wells at around 100 days (see C), water and oil pressures drop owing to the fact that water then can find an easy flow path to the production wells.

In Fig. 5, we show the results (phase pressures, velocities and saturations) of a compressible vertical three-phase model with a 400-day waterflooding displacement. Water is injected to displace oil and gas at both sides of the reservoir layer. It quickly fills the bottom part, then starts accumulating, see panel (C). Correspondingly, gas is displaced faster in the lower part than in the upper part because the reservoir layer is vertical. Gravity segregation is seen in the lower part where gas

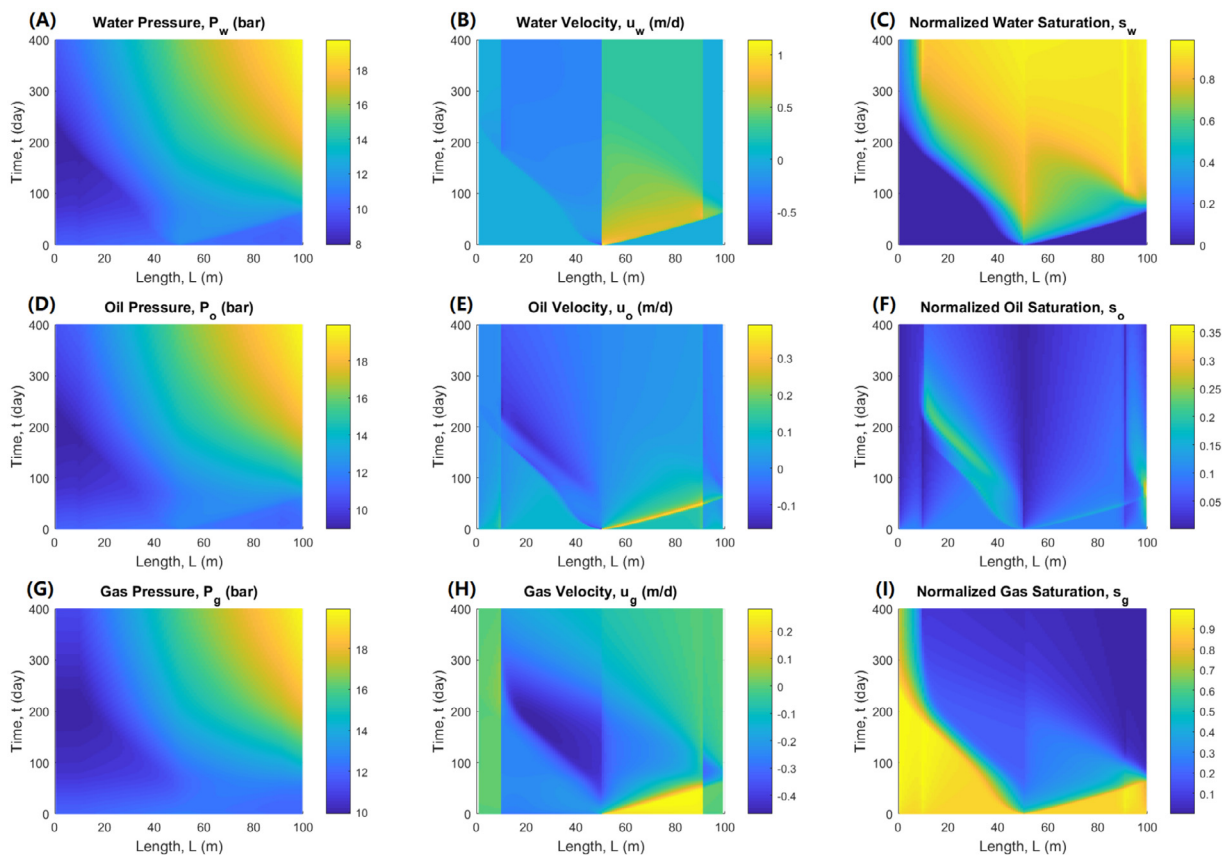


Fig. 5. Results of the vertical compressible three-phase model during a 400-day waterflooding period. The source term effects are identified in the velocity and saturation plots where production wells are located at 10 m and 90 m and injection well at 50 m. (A) Water pressure plot indicates that a lot of water flows toward the bottom and by that greatly increases the pressure in that region. (B) Due to the strong gravity effect water flows faster towards the bottom of layer compared the water displacement in the upper layer. (C) Normalized water saturation shows that water flows fastly to the bottom where it is accumulated before it begins to efficiently displace the upper part of the layer. (D) Oil pressure follows the similar behavior as water. (E) Water displaces the oil towards both sides from the center. However, at early time some oil in the upper part of the layer will move downwardly due to gravity. Later, the water front will displace oil upwardly. (F) The oil advancing front behaves similar as the water front. (G) Gas pressure behaves similar to the water pressure. (H) At an early stage gas is displaced towards the production well from the center. After water front has reached the bottom production well the whole bottom part of gas (50 m to 100 m) starts moving upwards. (I) Gas is recovered slowly in the upper part whereas gas recovery in the lower part consists of two stages: initially, gas is displaced by water to the bottom production well. Then, gas in the lower zone starts flowing upwardly.

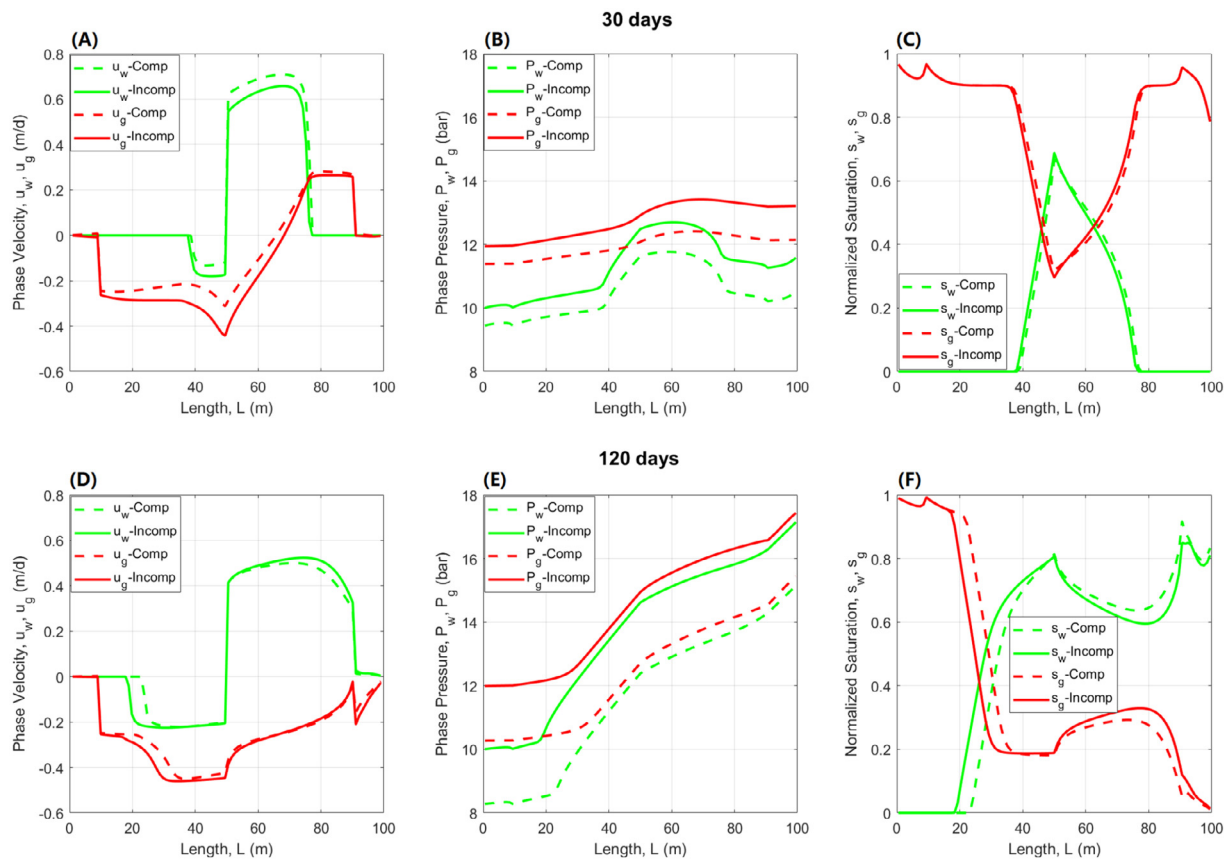


Fig. 6. Comparison between the compressible and incompressible model with vertical three-phase flow. (A,D) Phase velocity u_w and u_g for water and gas, respectively. (B,E) Pressure P_w and P_g for water and gas, respectively. The compressible model accounts for the fact that gas is significantly compressed and stores energy which is removed from the system as gas is produced. This gives rise to lower pressure profiles for the compressible case as compared to the incompressible case. This gives rise to a lower pressure level for the compressible model as compared to the incompressible. (C,F) Saturation s_w and s_g for water and gas, respectively.

is squeezed upwardly, see (H) and (I). In contrast to what is shown in Fig. 4G, gas pressure distribution shows a similar behavior as water and oil (higher at bottom and lower at top), see first column in Fig. 5. We refer to the figure text for more details.

4.1.1. Comparison of the compressible and incompressible models

We continue the discussion of the case shown in Fig. 5. In particular, we want to compare the behavior of the compressible and incompressible model. Constant density values $\rho_w = 1000 \text{ kg/m}^3$, $\rho_o = 800 \text{ kg/m}^3$ and $\rho_g = 18 \text{ kg/m}^3$ are used in the incompressible model.

Fig. 6 shows a comparison between the compressible and incompressible model after 30 and 120 days. (A) shows that at early stage the injected water in the compressible model prefers to displace gas in the lower part (high positive value) since water leads to higher pressure at the bottom such that the gas is compressed there. With compressed gas produced at the bottom and gas expanding in the upper part, gas will only slowly migrate towards the upper part resulting in comparably lower velocity (negative) in the compressible model. The velocity difference shown in (D) fits well with the saturation difference after 120 days. At the early time (30 days) the saturation differences are not distinct, see (C). However, after a long time (120 days) the differences are more significant, especially, in the water displacing part, see (F). This is due to the increasing phase pressure difference between compressible and incompressible model, see (B) and (E). The removal of compressed gas from the gas reservoir as (almost incompressible) water is injected clearly generates additional space for the water to fill which gives rise to a lower pressure.

4.2. The compressible three-phase model with a WAG experiment

In WAG processes, the injected water will migrate towards the bottom of the formation while the injected gas will flow upwardly. Therefore, counter-current flow occurs in the vertical direction of the reservoir due to the gravity segregation of water, oil and gas. Significant differences in terms of saturation distribution and producing GOR (gas-oil-ratio) have been reported between a conventional model and models that better can account for the mix of different flow regimes (co-current and counter-current). For example, in Sherafati and Jessen (2017) an explicit representation of flow transitions between co-current and counter-current flow was used to improve the design of WAG injection processes.

In this part, we conduct a water alternating gas (WAG) injection in a 1D reservoir (250 mD) layer which initially contains 90% oil and 10% water. The water and gas injection well is located at 50 m and two production wells are set at 10 m and 90 m. Gas is injected for the first 10 days followed by the water injection the next 10 days. Fluids can be produced in both production wells. The whole WAG experiment continues with an injection circulation of water and gas (each for 10 days).

Fig. 7 shows the result for a WAG injection process produced by the compressible three-phase vertical model where gravity segregation has a significant effect. From the simulation we see that pressure increases with time (first column in Fig. 7). Moreover, pressure values at the lower part of the layer are larger than at the upper part. Due to the density difference, water displaces oil faster in the bottom part, see (B) and (C). In addition, gas flows quickly towards the upper part of the reservoir

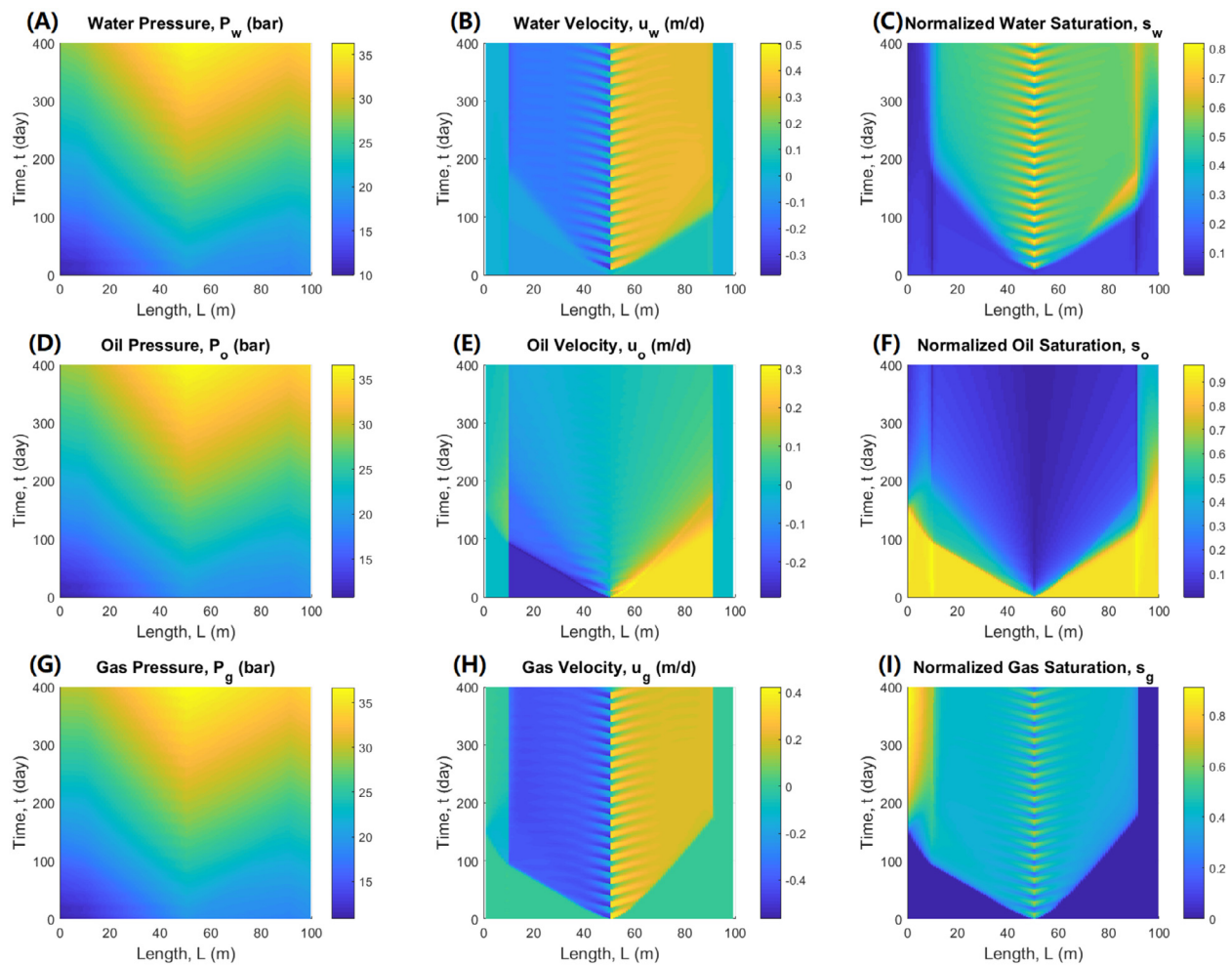


Fig. 7. Results of the vertical compressible three-phase model for a 400-day WAG injection process. The source term effects are visible in the velocity and saturation plots where production wells are located at 10 m and 90 m and injection well at 50 m. (A) A high pressure region in the layer center due to the water or gas injection and gravity effect. (B) Water advancing front implies that water flows faster towards the bottom of layer compared to the water displacement in the upper layer due to gravity segregation. (C) Water prefers to flow towards the bottom of layer where the edge region (90 m- 100 m) is also swept by water. (D) Oil pressure follows similar behavior as water pressure. (E) The upper part of oil is recovered faster than the lower part. (F) Due to the large density difference between oil and gas, the upper part oil is recovered very quickly, even for the edge region (0 m- 10 m). (G) Gas pressure. (H) Gas advancing front is fast in the upper part of layer because of the strong gravity segregation. (I) Gas reaches the bottom production well whereas a lot of gas is accumulated in the top region.

layer, see the saturation plots. In the upper part oil is recovered faster than in the lower part because of the larger density difference between gas and oil than the one between water and oil, see the second column in Fig. 7. We also observe that gas reaches the bottom production well but does not move further. This can be explained by the fact that gravity segregation effect overcomes the capillarity. However, a lot of gas is accumulated in the upper edge region (0 m- 10 m) due to the buoyancy force, see (I).

4.3. Comparison of compressible and incompressible three-phase models with WAG experiments

In this part, we compute solutions from incompressible three-phase models with same WAG injection process and compare the relevant results with those from the compressible three-phase model. Constant density values $\rho_w = 1000 \text{ kg/m}^3$, $\rho_o = 800 \text{ kg/m}^3$ and $\rho_g = 18 \text{ kg/m}^3$ are used in the incompressible model

Fig. 8 shows a comparison between the compressible and incompressible model of the vertical three-phase reservoir with a WAG process. Similar to what was observed in Fig. 6, differences are seen for

phase velocity, pressure and saturation. With increasing time, this difference will be enhanced, especially for the pressure. This is mainly due to the gas compressibility. See (B) and (E) and the figure text for more explanation. Because of the density difference water prefers to flow towards the bottom of the layer whereas gas moves faster towards the upper part of layer, see (C) and (F).

4.3.1. Effect of fluid-fluid interactions

Here we want to illustrate the impact from fluid-fluid interaction terms on the compressible model with a WAG process. Two situations are compared below: one with $I_{wo} = I_{wg} = I_{og} = 0 \text{ (Pa} \cdot \text{s)}^{-1}$ and one with $I_{wo} = I_{wg} = I_{og} = 5000 \text{ (Pa} \cdot \text{s)}^{-1}$.

Fig. 9 compares the results for the horizontal model for a WAG process with and without fluid-fluid interaction effect at 60 and 120 days. In (B) and (E), we observe that due to the fluid-fluid interaction, pressure is elevated compared with the case with no fluid-fluid interaction. The water velocity (A) and saturation profiles (C) show that water to a less extent displaces oil and instead flows through the original water channels when fluid-fluid interaction is included. The difference in the water saturation profiles between (C) and (F) is enhanced with time

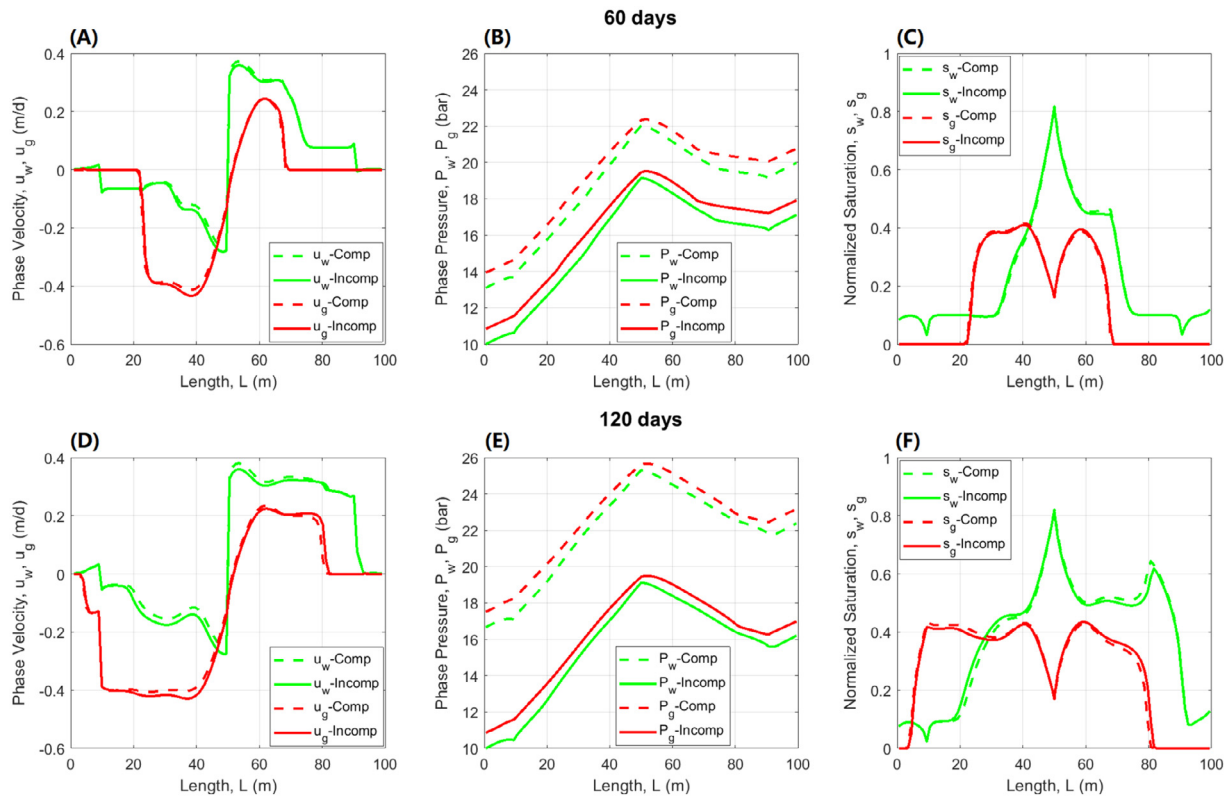


Fig. 8. Comparison between the compressible and incompressible model of the vertical three-phase reservoir with a WAG process. Results are shown after 60 and 120 days. (A) Gravity segregation results in a fast advancing front of gas in the upper part of layer and a fast advancing front of water in the lower part of layer. (B) Phase pressure in the compressible model is higher since the compressed gas wants to expand when it moves to a region with lower pressure but cannot expand due to the constrained space for gas. (C) Gas prefers to move towards the upper part of layer and water prefers to flow towards the lower part. (D) At 120 days, gas reaches the upper production well and water arrives at the bottom well. (E) Phase pressure in the compressible model increases with time compared with (B). (F) The difference between the two models is enhanced with time.

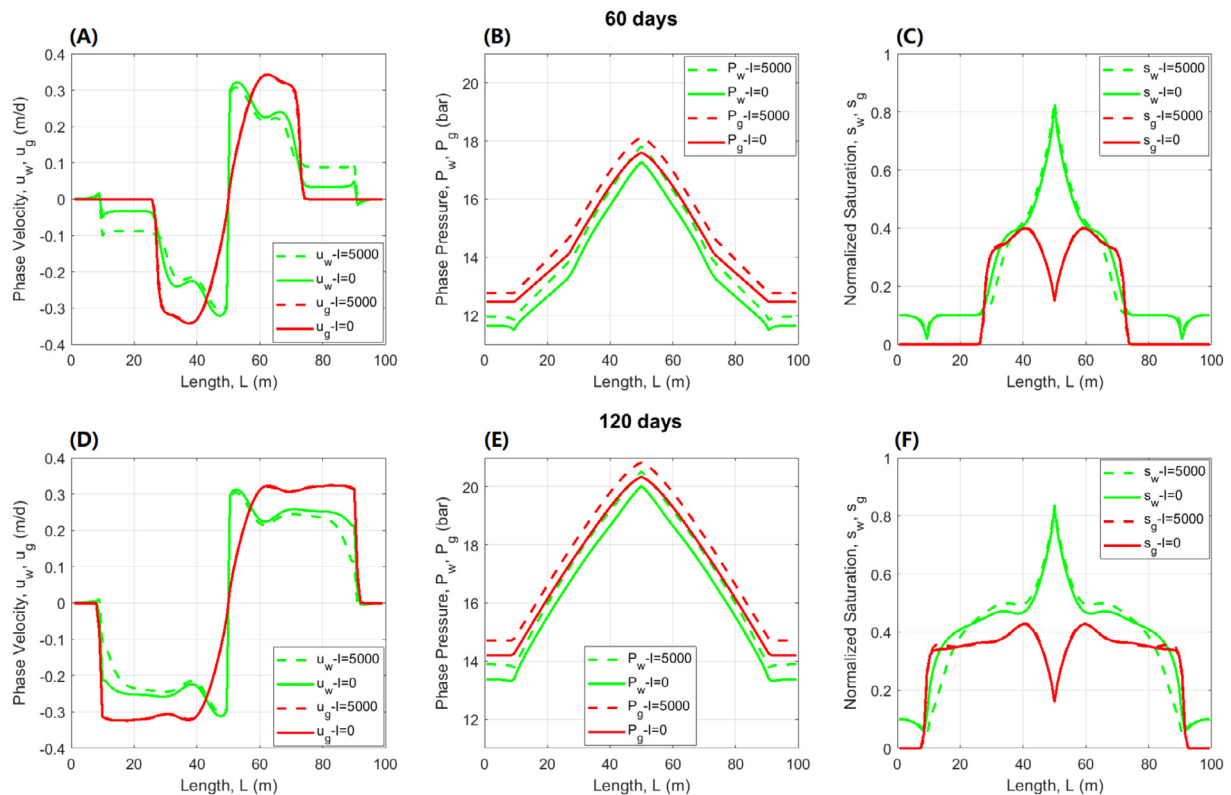


Fig. 9. Comparison for the horizontal compressible model for a WAG process with and without fluid-fluid interaction effects. The situation after 60 and 120 days are plotted. (A) Phase velocity at 60 days. (B) Phase pressure at 60 days. (C) Normalized saturation at 60 days. (D) Phase velocity at 120 days. (E) Phase pressure at 120 days. (F) Normalized saturation at 120 days.

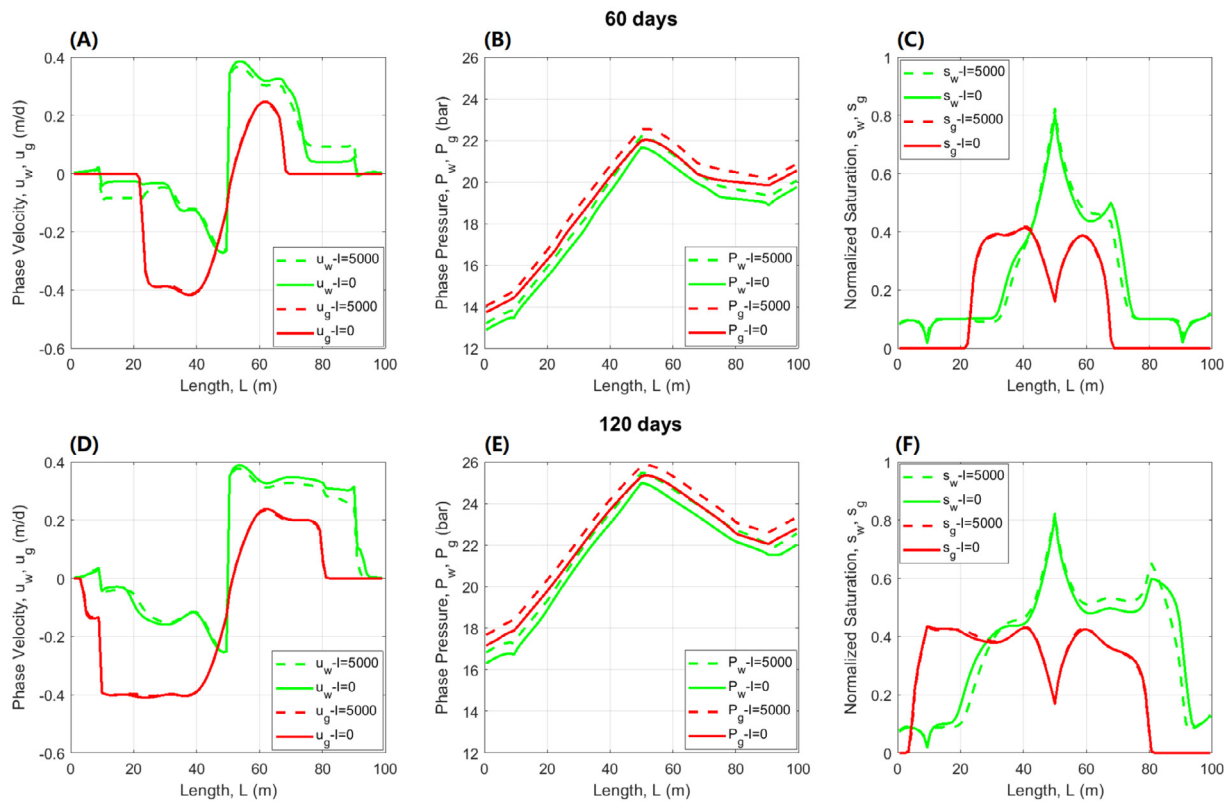


Fig. 10. Comparison of the vertical compressible model for a WAG process with and without fluid-fluid interaction effect at 60 and 120 days. (A) Phase velocity at 60 days. (B) Phase pressure at 60 days. (C) Normalized saturation at 60 days. (D) Phase velocity at 120 days. (E) Phase pressure at 120 days. (F) Normalized saturation at 120 days. Water tends to flow towards the lower part of layer due to the gravity segregation, resulting in a strong fluid-fluid interaction in the lower part of layer where the water saturation profiles clearly are affected, see (D) and (F).

due to the additional resistance force from the fluid-fluid interaction term.

Fig. 10 compares the results for the vertical model for a WAG process with and without fluid-fluid interaction effect at 60 and 120 days. Due to the density difference a large proportion of gas flows to the upper part of layer, see (C) and (F), and more of the water flows towards the bottom part of layer. As a result, differences are seen for the water velocity (A,D) and saturation (C,F) for the case with and without fluid-fluid interaction. Similar to Fig. 9, the build-up of the water front is less efficient for the case with fluid-fluid interaction since a larger portion of water tends to move through the original water channels (A).

5. Concluding remarks

We have presented a three-phase compressible and incompressible viscous model based on the mixture theory approach. The formulation represents an extension of the conventional Darcy-type formulations by including fluid-fluid viscous coupling effects. The three-phase flow model consists of a set of mass balance equations which are coupled to a set of momentum balance equations that involve both fluid-matrix, fluid-fluid interactions, and internal viscosity effects. Numerical schemes have been developed for both the compressible and incompressible model. Moreover, various waterflooding displacement scenar-

ios in a gas reservoir and WAG injection in an oil reservoir have been investigated to illustrate the effects of fluid compressibility and fluid-fluid viscous coupling. Main findings are:

- (i) The numerical schemes proposed in this paper appear to be robust and stable for simulation of various three-phase flow scenarios, both for the incompressible and compressible case;
- (ii) Comparison of the results for the compressible and incompressible model show that the differences between these two models can be significant, especially in the vertical case where the effect of gravity segregation is rather strong (see (F) in Fig. 6);
- (iii) The viscous coupling (fluid-fluid interaction) can have a significant effect on the results. A strong fluid-fluid viscous coupling results in a large resistance force for the flow of displacing fluid (water) such that: (a) Water prefers to move through the original water channels rather than displacing oil (see (A) and (C) in Figs. 9 and 10); (b) Water front is slow and builds up (see (F) in Figs. 9 and 10).

Declaration of Competing Interest

The authors declare that they have no known competing financial interests or personal relationships that could have appeared to influence the work reported in this paper.

Appendix A

From the three mass balance equations we get after multiplying the oil mass balance with $\rho_w \rho_g$, the water mass balance with $\rho_o \rho_g$ and the c mass balance with $\rho_w \rho_o$,

$$\begin{cases} (s_{wt} \rho_w + s_w \rho_{wt}) \rho_o \rho_g + \rho_o \rho_g (s_w \rho_w u_w)_x = -s_w \rho_w \rho_o \rho_g Q_p / \phi + \rho_w \rho_o \rho_g Q_{Iw} / \phi, \\ (s_{ot} \rho_o + s_o \rho_{ot}) \rho_w \rho_g + \rho_w \rho_g (s_o \rho_o u_o)_x = -s_o \rho_w \rho_o \rho_g Q_p / \phi, \\ (s_{gt} \rho_g + s_g \rho_{gt}) \rho_w \rho_o + \rho_w \rho_o (s_g \rho_g u_g)_x = -s_g \rho_w \rho_o \rho_g Q_p / \phi + \rho_w \rho_o \rho_g Q_{Ig} / \phi, \end{cases} \tag{5.34}$$

and summing the three resulting equations

$$f_1 + f_2 + f_3 = f_4, \tag{5.35}$$

where

$$\begin{aligned} f_1 &= s_{wt} \rho_w \rho_o \rho_g + s_{ot} \rho_w \rho_o \rho_g + s_{gt} \rho_w \rho_o \rho_g = \rho_w \rho_o \rho_g (s_{wt} + s_{ot} + s_{gt}) = 0, \\ f_2 &= s_w \rho_{wt} \rho_o \rho_g + s_o \rho_{ot} \rho_w \rho_g + s_g \rho_{gt} \rho_w \rho_o, \\ f_3 &= \rho_o \rho_g (s_w \rho_w u_w)_x + \rho_w \rho_g (s_o \rho_o u_o)_x + \rho_w \rho_o (s_g \rho_g u_g)_x, \\ f_4 &= -s_w \rho_w \rho_o \rho_g Q_p / \phi + \rho_w \rho_o \rho_g Q_{Iw} / \phi - s_o \rho_w \rho_o \rho_g Q_p / \phi - s_g \rho_w \rho_o \rho_g Q_p / \phi + \rho_w \rho_o \rho_g Q_{Ig} / \phi \\ &= \rho_w \rho_o \rho_g (Q_{Iw} + Q_{Ig} - Q_p) / \phi. \end{aligned}$$

Here we want to focus on dealing with expression f_2 .

$$f_2 = s_w \rho_o \rho_g \frac{P_{wt}}{C_w} + s_o \rho_w \rho_g \frac{P_{ot}}{C_o} + s_g \rho_w \rho_o \frac{P_{gt}}{C_g}, \tag{5.36}$$

$$\begin{aligned} P_{ot} &= (P_w + \Delta P_{ow})_t = P_{wt} + \Delta P'_{ow} s_{wt}, \\ P_{gt} &= (P_w + \Delta P_{ow} + \Delta P_{go})_t = P_{wt} + \Delta P'_{ow} s_{wt} + \Delta P'_{go} s_{gt} \quad \text{and} \\ s_{gt} &= -(s_{wt} + s_{ot}) = -\left(s_{wt} + \frac{n_{ot}}{\rho_o} - \frac{n_o}{C_o \rho_o^2} P_{ot}\right) = -\left(s_{wt} + \frac{n_{ot}}{\rho_o} - \frac{n_o}{C_o \rho_o^2} (P_{wt} + \Delta P'_{ow} s_{wt})\right). \end{aligned} \tag{5.37}$$

Therefore we have

$$f_2 = \left(\kappa \rho_w + \frac{s_w \rho_o \rho_g}{C_w}\right) P_{wt} + \kappa \rho_w \Delta P'_{ow} s_{wt} - \frac{s_g \rho_w \rho_o}{C_g} \Delta P'_{go} s_{wt} - \frac{s_g \rho_w}{C_g} n_{ot}; \tag{5.38}$$

where

$$\kappa = \frac{s_o \rho_g}{C_o} + \frac{s_g \rho_o}{C_g} + \frac{s_g s_o}{C_o C_g}. \tag{5.39}$$

Clearly,

$$s_{wt} = \left(\frac{n_w}{\rho_w}\right)_t = \frac{1}{\rho_w} n_{wt} - \frac{m}{\rho_w^2} \rho_{wt} = \frac{1}{\rho_w} n_{wt} - \frac{m}{C_w \rho_w^2} P_{wt}.$$

Consequently,

$$\begin{aligned} f_2 &= \left[\kappa \rho_w + \frac{s_w \rho_o \rho_g}{C_w} - \frac{s_w}{C_w} \left(\kappa \Delta P'_{ow} - \frac{s_g \rho_o}{C_g} \Delta P'_{go}\right)\right] P_{wt} - \left(\kappa \Delta P'_{ow} - \frac{s_g \rho_o}{C_g} \Delta P'_{go}\right) (s_w \rho_w u_w)_x \\ &\quad + \frac{s_g \rho_w}{C_g} (s_o \rho_o u_o)_x - \frac{s_g \rho_w}{C_g} s_o \rho_o Q_p - (\rho_w s_w Q_p - \rho_w Q_{Iw}) \left(\kappa \Delta P'_{ow} - \frac{s_g \rho_o}{C_g} \Delta P'_{go}\right) \end{aligned} \tag{5.40}$$

Since that $f_1 = 0$, (5.35) will have the following form:

$$\begin{aligned} &\left[\kappa \rho_w + \frac{s_w \rho_o \rho_g}{C_w} - \frac{s_w}{C_w} \left(\kappa \Delta P'_{ow} - \frac{s_g \rho_o}{C_g} \Delta P'_{go}\right)\right] P_{wt} + \left(\rho_o \rho_g + \frac{s_g \rho_o}{C_g} \Delta P'_{go} - \kappa \Delta P'_{ow}\right) (s_w \rho_w u_w)_x \\ &\quad + \left(\rho_w \rho_g + \frac{s_g \rho_w}{C_g}\right) (s_o \rho_o u_o)_x + \rho_w \rho_o (s_g \rho_g u_g)_x = \rho_w \rho_o \rho_g (Q_{Iw} + Q_{Ig} - Q_p) / \phi + \frac{s_g \rho_w}{C_g} s_o \rho_o Q_p / \phi \\ &\quad + (\rho_w s_w Q_p / \phi - \rho_w Q_{Iw} / \phi) \left(\kappa \Delta P'_{ow} + \frac{s_g \rho_o}{C_g} \Delta P'_{go}\right). \end{aligned} \tag{5.41}$$

The upper equation can be reformulated to be

$$P_{wt} + \tilde{\eta}_1 (n_w u_w)_x + \tilde{\eta}_2 (n_o u_o)_x + \tilde{\eta}_3 (n_g u_g)_x = \tilde{\eta}_4 Q_p / \phi + \tilde{\eta}_5 Q_{Iw} / \phi + \tilde{\eta}_6 Q_{Ig} / \phi; \tag{5.42}$$

where

$$\begin{aligned}
 \eta &= \kappa \rho_w + \frac{s_w \rho_o \rho_g}{C_w} - \frac{s_w}{C_w} \left(\kappa \Delta P'_{ow} - \frac{s_g \rho_o}{C_g} \Delta P'_{go} \right) \\
 \tilde{\eta}_1 &= \frac{1}{\eta} \left(\rho_o \rho_g + \frac{s_g \rho_o}{C_g} \Delta P'_{go} - \kappa \Delta P'_{ow} \right) \\
 \tilde{\eta}_2 &= \frac{1}{\eta} \left(\rho_w \rho_g + \frac{s_g \rho_w}{C_g} \right) \\
 \tilde{\eta}_3 &= \frac{1}{\eta} \rho_w \rho_o \\
 \tilde{\eta}_4 &= \frac{1}{\eta} \left[\frac{s_g \rho_w}{C_g} s_o \rho_o + \rho_w s_w \left(\kappa \Delta P'_{ow} - \frac{s_g \rho_o}{C_g} \Delta P'_{go} \right) - \rho_w \rho_o \rho_g \right] \\
 \tilde{\eta}_5 &= \frac{1}{\eta} \left[\rho_w \rho_o \rho_g - \rho_w \left(\kappa \Delta P'_{ow} - \frac{s_g \rho_o}{C_g} \Delta P'_{go} \right) \right] \\
 \tilde{\eta}_6 &= \frac{1}{\eta} \rho_w \rho_o \rho_g.
 \end{aligned} \tag{5.43}$$

Remark 5.1. $\Delta P'_{ow}$ is always non-positive and $\Delta P'_{go}$ non-negative.

Appendix B. Numerical discretization of compressible version

We develop a numerical scheme for this general three-fluid flow model in a 1D setting. The proposed numerical methods are described separately for the compressible (Appendix B) and dummyTXdummy-(incompressible (Appendix C) model.

B1. A semi-discrete scheme for the compressible model

We consider a slight reformulation of the model where we shall make use of the pressure evolution Eq. (5.42). This will be convenient to account for the highly nonlinear coupling between the mass and momentum equations through the pressure terms. It also makes the discretization of the compressible and incompressible model consistent. The original model takes the form with $(n_w, n_o, n_g, u_w, u_o, u_g)$ as the main variables:

$$\begin{aligned}
 (\phi n_w)_t + (\phi n_w u_w)_x &= -n_w Q_p + \rho_w Q_{Iw}, & n_w &= s_w \rho_w \\
 (\phi n_o)_t + (\phi n_o u_o)_x &= -n_o Q_p, & n_o &= s_o \rho_o \\
 (\phi n_g)_t + (\phi n_g u_g)_x &= -n_g Q_p + \rho_g Q_{Ig}, & n_g &= s_g \rho_g \\
 s_w(P_w)_x &= -\hat{k}_w u_w - \hat{k}_{wo}(u_w - u_o) - \hat{k}_{wg}(u_w - u_g) + n_w g + \epsilon_w(n_w u_{wx})_x, \\
 s_o(P_o)_x &= -\hat{k}_o u_o - \hat{k}_{wo}(u_o - u_w) - \hat{k}_{og}(u_o - u_g) + n_o g + \epsilon_o(n_o u_{ox})_x, \\
 s_g(P_g)_x &= -\hat{k}_g u_g - \hat{k}_{wg}(u_g - u_w) - \hat{k}_{og}(u_g - u_o) + n_g g + \epsilon_g(n_g u_{gx})_x, \\
 \Delta P_{ow}(s_w) &= P_o - P_w, & \Delta P_{go}(s_g) &= P_g - P_o.
 \end{aligned} \tag{5.44}$$

Note that we may rewrite the model in the following equivalent form with $(n_w, n_o, P_w, u_w, u_o, u_g)$ as the main variables

$$\begin{aligned}
 (\phi n_w)_t + (\phi n_w u_w)_x &= -n_w Q_p + \rho_w Q_{Iw}, \\
 (\phi n_o)_t + (\phi n_o u_o)_x &= -n_o Q_p, \\
 P_{wt} + \tilde{\eta}_1(n_w u_w)_x + \tilde{\eta}_2(n_o u_o)_x + \tilde{\eta}_3(n_g u_g)_x &= \tilde{\eta}_4 Q_p / \phi + \tilde{\eta}_5 Q_{Iw} / \phi + \tilde{\eta}_6 Q_{Ig} / \phi, \\
 s_w(P_w)_x &= -\hat{k}_w u_w - \hat{k}_{wo}(u_w - u_o) - \hat{k}_{wg}(u_w - u_g) - n_w g + \epsilon_w(n_w u_{wx})_x, \\
 s_o(P_w + \Delta P_{ow})_x &= -\hat{k}_o u_o - \hat{k}_{wo}(u_o - u_w) - \hat{k}_{og}(u_o - u_g) - n_o g + \epsilon_o(n_o u_{ox})_x, \\
 s_g(P_w + \Delta P_{ow} + \Delta P_{go})_x &= -\hat{k}_g u_g - \hat{k}_{wg}(u_g - u_w) - \hat{k}_{og}(u_g - u_o) - n_g g + \epsilon_g(n_g u_{gx})_x, \\
 \Delta P_{ow}(s_w) &= P_o - P_w, & \Delta P_{go}(s_g) &= P_g - P_o.
 \end{aligned} \tag{5.45}$$

Here n_g is determined by

$$\begin{aligned}
 n_g &= s_g \rho_g(P_g) = (1 - s_w - s_o) \rho_g(P_g) \\
 &= \left(1 - \frac{n_w}{\rho_w(P_w)} - \frac{n_o}{\rho_o(P_o)} \right) \rho_g(P_g) = n_g(n_w, n_o, P_w),
 \end{aligned} \tag{5.46}$$

where $P_o = P_o(s_w, P_w) = P_o(n_w, P_w)$ and $P_g = P_g(s_w, s_o, P_w) = P_g(n_w, n_o, P_w)$. We may solve (5.45) on our domain Ω with boundary conditions

$$u_w|_{\partial\Omega} = u_o|_{\partial\Omega} = u_g|_{\partial\Omega} = 0 \tag{5.47}$$

and initial condition

$$\begin{aligned}
 n_w(x, t = 0) &= n_{w0}(x), & n_o(x, t = 0) &= n_{o0}(x), \\
 n_g(x, t = 0) &= n_{g0}(x), & P_w(x = 0, t = 0) &= P_{wL}.
 \end{aligned} \tag{5.48}$$

System of ODEs

We consider the domain $\Omega = [0, 1]$ and introduce a grid of N_x cells with nodes x_j placed at the center of the cells

$$x_1 = \frac{1}{2} \Delta x, \quad x_2 = \left(1 + \frac{1}{2} \right) \Delta x, \quad \dots, \quad x_j = \left(j - \frac{1}{2} \right) \Delta x, \quad \dots, \quad x_{N_x} = \left(N_x - \frac{1}{2} \right) \Delta x$$

and cell interfaces $x_{j+1/2}$ at the cell interfaces

$$x_{1/2} = 0, \quad x_{3/2} = \Delta x, \quad \dots, \quad x_{j+1/2} = j\Delta x, \quad \dots, \quad x_{N_x+1/2} = N_x\Delta x = 1,$$

where $\Delta x = 1/N_x$. We introduce the approximate masses $\{n_{w,j}(t)\}_{j=1}^{N_x}$, $\{n_{o,j}(t)\}_{j=1}^{N_x}$, and $\{n_{g,j}(t)\}_{j=1}^{N_x}$ associated with the nodes $\{x_j\}_{j=1}^{N_x}$ whereas the approximate velocities $\{u_{w,j+1/2}\}_{j=0}^{N_x}$, $\{u_{o,j+1/2}\}_{j=0}^{N_x}$, and $\{u_{g,j+1/2}\}_{j=0}^{N_x}$ are associated with the cell interfaces $\{x_{j+1/2}\}_{j=0}^{N_x}$.

Step 1: Mass transport

We solve for $n_{w,j}(t)$ by considering the following ODE: for the water phase,

$$\dot{n}_{w,j} + \frac{1}{\Delta x}([n_w u_w]_{j+1/2} - [n_w u_w]_{j-1/2}) = -n_{w,j} Q_{p,j} / \phi + \rho_{w,j} Q_{Iw,j} / \phi, \quad n_w = s_w \rho_w \tag{5.49}$$

where

$$[n_w u_w]_{j+1/2} = \begin{cases} n_{w,j} u_{w,j+1/2}, & \text{if } u_{w,j+1/2} \geq 0; \\ n_{w,j+1} u_{w,j+1/2}, & \text{if } u_{w,j+1/2} < 0. \end{cases} \tag{5.50}$$

This can also be expressed as

$$[n_w u_w]_{j+1/2} = \frac{n_{w,j} + n_{w,j+1}}{2} u_{w,j+1/2} - \frac{1}{2} (n_{w,j+1} - n_{w,j}) |u_{w,j+1/2}|$$

for the oil phase,

$$\dot{n}_{o,j} + \frac{1}{\Delta x}([n_o u_o]_{j+1/2} - [n_o u_o]_{j-1/2}) = -n_{o,j} Q_{p,j} / \phi, \quad n_o = s_o \rho_o \tag{5.51}$$

where

$$[n_o u_o]_{j+1/2} = \begin{cases} n_{o,j} u_{o,j+1/2}, & \text{if } u_{o,j+1/2} \geq 0; \\ n_{o,j+1} u_{o,j+1/2}, & \text{if } u_{o,j+1/2} < 0. \end{cases} \tag{5.52}$$

Remark 5.2. It should be pointed out that $Q_{p,j} = \frac{\bar{Q}_p}{\sigma}$ and $Q_{Iw,j} = \frac{\bar{Q}_{Iw}}{\sigma}$ (where j refers to a grid cell which contains a producer/injector) due to the fact that production Q_p or injection Q_{Iw} in (5.44) is interpreted as a value at a point location. The width of the small region associated with the injector and producer is $\sigma = \Delta x$ consistent with (4.33). This also applies for $Q_{Ig,j}$ in (5.53), that is to say, $Q_{Ig,j} = \frac{\bar{Q}_{Ig}}{\sigma}$.

Step 2: Computation of velocities and pressure

Next, we solve for $P_{w,j}(t)$ and $u_{w,j+1/2}(t)$, $u_{o,j+1/2}(t)$ and $u_{g,j+1/2}(t)$ by considering the following ODE system:

$$\begin{aligned} \dot{P}_{w,j} + \tilde{\eta}_{1,j} \frac{1}{\Delta x}([n_w u_w]_{j+1/2} - [n_w u_w]_{j-1/2}) + \tilde{\eta}_{2,j} \frac{1}{\Delta x}([n_o u_o]_{j+1/2} - [n_o u_o]_{j-1/2}) \\ + \tilde{\eta}_{3,j} \frac{1}{\Delta x}([n_g u_g]_{j+1/2} - [n_g u_g]_{j-1/2}) = \tilde{\eta}_{4,j} Q_{p,j} / \phi + \tilde{\eta}_{5,j} Q_{Iw,j} / \phi + \tilde{\eta}_{6,j} Q_{Ig,j} / \phi \end{aligned} \tag{5.53}$$

which is combined with the momentum balance equations

$$\begin{aligned} s_{w,j+1/2} \frac{1}{\Delta x} (P_{w,j+1} - P_{w,j}) &= -\hat{k}_{w,j+1/2} u_{w,j+1/2} - \hat{k}_{wo,j+1/2} (u_{w,j+1/2} - u_{o,j+1/2}) - \hat{k}_{wg,j+1/2} (u_{w,j+1/2} - u_{g,j+1/2}) \\ &\quad - g n_{w,j+1/2} + \epsilon_w \frac{1}{\Delta x^2} (n_{w,j+1} [u_{w,j+3/2} - u_{w,j+1/2}] - n_{w,j} [u_{w,j+1/2} - u_{w,j-1/2}]) \\ s_{o,j+1/2} \frac{1}{\Delta x} (P_{w,j+1} - P_{w,j}) &= -s_{o,j+1/2} \frac{1}{\Delta x} (\Delta P_{ow,j+1} - \Delta P_{ow,j}) \\ &\quad - \hat{k}_{o,j+1/2} u_{o,j+1/2} - \hat{k}_{wo,j+1/2} (u_{o,j+1/2} - u_{w,j+1/2}) - \hat{k}_{og,j+1/2} (u_{o,j+1/2} - u_{g,j+1/2}) \\ &\quad - g n_{o,j+1/2} + \epsilon_o \frac{1}{\Delta x^2} (n_{o,j+1} [u_{o,j+3/2} - u_{o,j+1/2}] - n_{o,j} [u_{o,j+1/2} - u_{o,j-1/2}]) \\ s_{g,j+1/2} \frac{1}{\Delta x} (P_{w,j+1} - P_{w,j}) &= -s_{g,j+1/2} \frac{1}{\Delta x} (\Delta P_{ow,j+1} - \Delta P_{ow,j} + \Delta P_{go,j+1} - \Delta P_{go,j}) \\ &\quad - \hat{k}_{g,j+1/2} u_{g,j+1/2} - \hat{k}_{wg,j+1/2} (u_{g,j+1/2} - u_{w,j+1/2}) - \hat{k}_{og,j+1/2} (u_{g,j+1/2} - u_{o,j+1/2}) - g c_{g,j+1/2} \\ &\quad + \epsilon_g \frac{1}{\Delta x^2} (c_{g,j+1} [u_{g,j+3/2} - u_{g,j+1/2}] - n_{g,j} [u_{g,j+1/2} - u_{g,j-1/2}]) \end{aligned} \tag{5.54}$$

Here we note that the average $s_{w,j+1/2}$ in (5.54) is based on upwind relatively $u_{w,j+1/2}$

$$s_{w,j+1/2} = \begin{cases} s_{w,j}, & \text{if } u_{w,j+1/2} > 0; \\ \frac{s_{w,j} + s_{w,j+1}}{2}, & \text{if } u_{w,j+1/2} = 0; \\ s_{w,j+1}, & \text{if } u_{w,j+1/2} < 0. \end{cases} \tag{5.55}$$

Similarly, for $s_{o,j+1/2}$, $s_{g,j+1/2}$ and for the interaction terms $\hat{k}_{w,j+1/2}$, $\hat{k}_{o,j+1/2}$ and $\hat{k}_{g,j+1/2}$. For $\hat{k}_{wo,j+1/2}$, $\hat{k}_{og,j+1/2}$ and $\hat{k}_{wg,j+1/2}$ we use the following method:

$$\hat{k}_{wo,j+1/2} = \begin{cases} \hat{k}_{wo,j}, & \text{if } u_{w,j+1/2} > 0 \& u_{o,j+1/2} > 0; \\ \frac{\hat{k}_{wo,j} + \hat{k}_{wo,j+1}}{2}, & \text{if } u_{w,j+1/2} u_{o,j+1/2} \leq 0; \\ \hat{k}_{wo,j+1}, & \text{if } u_{w,j+1/2} < 0 \& u_{o,j+1/2} < 0. \end{cases} \tag{5.56}$$

$\hat{k}_{wg,j+1/2}$ and $\hat{k}_{og,j+1/2}$ are also approximated using the similar way. On the other hand, $[n_w u_w]_{j+1/2}$, $[n_o u_o]_{j+1/2}$ and $[n_g u_g]_{j+1/2}$ appearing in (5.53) employ upwind as described in (5.50).

Now, we are in a position where we can describe a fully discrete model.

B2. A fully discrete scheme

We assume that we have given $(n_{w,j}^k, n_{o,j}^k, P_{w,j}^k, u_{w,j}^k, u_{o,j}^k, u_{g,j}^k)$. We then compute the approximate solution at time t^{k+1} expressed by $(n_{w,j}^{k+1}, n_{o,j}^{k+1}, P_{w,j}^{k+1}, u_{w,j}^{k+1}, u_{o,j}^{k+1}, u_{g,j}^{k+1})$ as follows:

Step 1: Mass transport

$$\frac{n_{w,j}^{k+1} - n_{w,j}^k}{\Delta t} + \frac{1}{\Delta x} ([n_w u_w]_{j+1/2}^k - [n_w u_w]_{j-1/2}^k) = -n_{w,j}^k Q_{p,j}^k / \phi + \rho_{w,j}^k Q_{1w,j}^k / \phi \tag{5.57}$$

where

$$[n_w u_w]_{j+1/2}^k = \begin{cases} n_{w,j}^k u_{w,j+1/2}^k, & \text{if } u_{w,j+1/2}^k \geq 0; \\ n_{w,j+1}^k u_{w,j+1/2}^k, & \text{if } u_{w,j+1/2}^k < 0. \end{cases} \tag{5.58}$$

$$\frac{n_{o,j}^{k+1} - n_{o,j}^k}{\Delta t} + \frac{1}{\Delta x} ([n_o u_o]_{j+1/2}^k - [n_o u_o]_{j-1/2}^k) = -n_{o,j}^k Q_{p,j}^k / \phi \tag{5.59}$$

where

$$[n_o u_o]_{j+1/2}^k = \begin{cases} n_{o,j}^k u_{o,j+1/2}^k, & \text{if } u_{w,j+1/2}^k \geq 0; \\ n_{o,j+1}^k u_{o,j+1/2}^k, & \text{if } u_{w,j+1/2}^k < 0. \end{cases} \tag{5.60}$$

Having computed $n_{w,j}^{k+1}$ and $n_{o,j}^{k+1}$ we can compute an updated water saturation $s_{w,j}^{k+1/2}$ and $s_{o,j}^{k+1/2}$ given by

$$s_{w,j}^{k+1/2} = \frac{n_{w,j}^{k+1}}{\rho_w(P_{w,j}^{k+1/2})}, \quad s_{o,j}^{k+1/2} = \frac{n_{o,j}^{k+1}}{\rho_o(P_{o,j}^{k+1/2})} = \frac{n_{o,j}^{k+1}}{\rho_o(P_{w,j}^{k+1/2} + \Delta P_{ow}(s_{w,j}^{k+1/2}))}. \tag{5.61}$$

Similarly, we compute updated mass $n_{g,j}^{k+1/2}$ and $P_{g,j}^{k+1/2}$ needed to evaluate coefficients in the next step.

Step 2: Computation of velocities and pressure

Next, we solve simultaneously for $P_{w,j}^{k+1}$ and $u_{w,j+1/2}^{k+1}$, $u_{o,j+1/2}^{k+1}$ and $u_{g,j+1/2}^{k+1}$ by considering the following algebraic system

$$\begin{aligned} &\frac{P_{w,j}^{k+1} - P_{w,j}^k}{\Delta t} + \tilde{\eta}_{1,j}^{k+1/2} \frac{1}{\Delta x} ([n_w^{k+1} u_w^{k+1}]_{j+1/2} - [n_w^{k+1} u_w^{k+1}]_{j-1/2}) + \tilde{\eta}_{2,j}^{k+1/2} \frac{1}{\Delta x} ([n_o^{k+1} u_o^{k+1}]_{j+1/2} \\ &\quad - [n_o^{k+1} u_o^{k+1}]_{j-1/2}) + \tilde{\eta}_{3,j}^{k+1/2} \frac{1}{\Delta x} ([n_g^{k+1/2} u_g^{k+1}]_{j+1/2} - [n_g^{k+1/2} u_g^{k+1}]_{j-1/2}) \\ &\tilde{\eta}_{4,j}^{k+1/2} Q_{p,j}^k / \phi + \tilde{\eta}_{5,j}^{k+1/2} Q_{1w,j}^k / \phi + \tilde{\eta}_{6,j}^{k+1/2} Q_{1g,j}^k / \phi \end{aligned} \tag{5.62}$$

which is combined with the momentum balance equations

$$\begin{aligned} s_{w,j+1/2}^{k+1/2} \frac{1}{\Delta x} (P_{w,j+1}^{k+1} - P_{w,j}^{k+1}) &= -\hat{k}_{w,j+1/2}^{k+1/2} u_{w,j+1/2}^{k+1} - \hat{k}_{wo,j+1/2}^{k+1/2} (u_{w,j+1/2}^{k+1/2} - u_{o,j+1/2}^{k+1/2}) - \hat{k}_{wg,j+1/2}^{k+1/2} (u_{w,j+1/2}^{k+1/2} - u_{g,j+1/2}^{k+1/2}) \\ &\quad - n_{w,j+1/2}^{k+1} g + \epsilon_w \frac{1}{\Delta x^2} (n_{w,j+1}^{k+1} [u_{w,j+3/2}^{k+1} - u_{w,j+1/2}^{k+1}] - n_{w,j}^{k+1} [u_{w,j+1/2}^{k+1} - u_{w,j-1/2}^{k+1}]) \\ s_{o,j+1/2}^{k+1/2} \frac{1}{\Delta x} (P_{w,j+1}^{k+1} - P_{w,j}^{k+1}) &= -s_{o,j+1/2}^{k+1/2} \frac{1}{\Delta x} (\Delta P_{ow,j+1}^{k+1/2} - \Delta P_{ow,j}^{k+1/2}) \\ &\quad - \hat{k}_{oj+1/2}^{k+1/2} u_{o,j+1/2}^{k+1} - \hat{k}_{wo,j+1/2}^{k+1/2} (u_{o,j+1/2}^{k+1} - u_{w,j+1/2}^{k+1}) - \hat{k}_{og,j+1/2}^{k+1/2} (u_{o,j+1/2}^{k+1} - u_{g,j+1/2}^{k+1}) \\ &\quad - n_{o,j+1/2}^{k+1} g + \epsilon_o \frac{1}{\Delta x^2} (n_{o,j+1}^{k+1} [u_{o,j+3/2}^{k+1} - u_{o,j+1/2}^{k+1}] - n_{o,j}^{k+1} [u_{o,j+1/2}^{k+1} - u_{o,j-1/2}^{k+1}]) \\ s_{g,j+1/2}^{k+1/2} \frac{1}{\Delta x} (P_{w,j+1}^{k+1} - P_{w,j}^{k+1}) &= -s_{g,j+1/2}^{k+1/2} \frac{1}{\Delta x} (\Delta P_{ow,j+1}^{k+1/2} - \Delta P_{ow,j}^{k+1/2} + \Delta P_{go,j+1}^{k+1/2} - \Delta P_{go,j}^{k+1/2}) \\ &\quad - \hat{k}_{gj+1/2}^{k+1/2} u_{g,j+1/2}^{k+1} - \hat{k}_{wg,j+1/2}^{k+1/2} (u_{g,j+1/2}^{k+1} - u_{w,j+1/2}^{k+1}) - \hat{k}_{og,j+1/2}^{k+1/2} (u_{g,j+1/2}^{k+1} - u_{o,j+1/2}^{k+1}) \\ &\quad - n_{g,j+1/2}^{k+1} g + \epsilon_g \frac{1}{\Delta x^2} (n_{g,j+1}^{k+1} [u_{g,j+3/2}^{k+1} - u_{g,j+1/2}^{k+1}] - n_{g,j}^{k+1} [u_{g,j+1/2}^{k+1} - u_{g,j-1/2}^{k+1}]) \end{aligned} \tag{5.63}$$

Equipped with $(P_{w,j}^{k+1}, u_{w,j+1/2}^{k+1}, u_{o,j+1/2}^{k+1}, u_{g,j+1/2}^{k+1})$ we can now update the saturation

$$s_{w,j}^{k+1} = \frac{n_{w,j}^{k+1}}{\rho_w(P_{w,j}^{k+1})}, \quad s_{o,j}^{k+1} = \frac{n_{o,j}^{k+1}}{\rho_o(P_{o,j}^{k+1})} = \frac{n_{o,j}^{k+1}}{\rho_o(P_{w,j}^{k+1} + \Delta P_{ow,j}(s_{w,j}^{k+1}))} \tag{5.64}$$

from which we also compute the updated gas mass $n_{g,j}^{k+1}$ via (5.46). If necessary, we may repeat step 2 to improve the accuracy before we proceed to next time level.

Remark 5.3. The upwind discretization of $[n_w^{k+1} u_w^{k+1}]_{j+1/2}$, $[n_o^{k+1} u_o^{k+1}]_{j+1/2}$ and $[n_g^{k+1/2} u_g^{k+1}]_{j+1/2}$ appearing in (5.62) are based on "old" velocities $u_{w,j+1/2}^k$, $u_{o,j+1/2}^k$ and $u_{g,j+1/2}^k$.

Remark 5.4. For the higher dimensional case mentioned in Remark 3.1, we can use a similar way to solve two mass equations as step 1 for the 1D case. Then compute pressure and velocities by using a 2D pressure evolution equation similar to the one derived for the 1D case in Appendix A together with six momentum equations for three phases in x and y direction.

Appendix C. Numerical discretization of incompressible version

We first describe a semi-discrete approximation of the incompressible version of model (3.11).

C1. A semidiscrete scheme for the incompressible model

When fluids are incompressible the model (5.45) takes the form

$$\begin{aligned}
 (s_w)_t + (s_w u_w)_x &= -s_w Q_p / \phi + Q_{Iw} / \phi, \\
 (s_o)_t + (s_o u_o)_x &= -s_o Q_p / \phi, \\
 (s_w u_w + s_o u_o + s_g u_g)_x &= -Q_p / \phi + Q_{Iw} / \phi + Q_{Ig} / \phi, \\
 s_w (P_w)_x &= -\hat{k}_{lw} u_w - \hat{k}_{wo} (u_w - u_o) - \hat{k}_{wg} (u_w - u_g) + n_w g + \epsilon_w \rho_w (s_w u_{wx})_x, \\
 s_o (P_o)_x &= -\hat{k}_{lo} u_o - \hat{k}_{wo} (u_o - u_w) - \hat{k}_{og} (u_o - u_g) + n_o g + \epsilon_o \rho_o (s_o u_{ox})_x, \\
 s_g (P_g)_x &= -\hat{k}_{lg} u_g - \hat{k}_{wg} (u_g - u_w) - \hat{k}_{og} (u_g - u_o) + n_g g + \epsilon_g \rho_g (s_g u_{gx})_x, \\
 \Delta P_{ow} (s_w) &= P_o - P_w, \quad \Delta P_{go} (s_g) = P_g - P_o.
 \end{aligned} \tag{5.65}$$

Step 1: Mass transport

$$\dot{s}_{w,j} + \frac{1}{\Delta x} ([s_w u_w]_{j+1/2} - [s_w u_w]_{j-1/2}) = -s_{w,j} Q_{p,j} / \phi + Q_{Iw,j} / \phi \tag{5.66}$$

where

$$[s_w u_w]_{j+1/2} = \begin{cases} s_{w,j} u_{w,j+1/2}, & \text{if } u_{w,j+1/2} \geq 0; \\ s_{w,j+1} u_{w,j+1/2}, & \text{if } u_{w,j+1/2} < 0. \end{cases} \tag{5.67}$$

$$\dot{s}_{o,j} + \frac{1}{\Delta x} ([s_o u_o]_{j+1/2} - [s_o u_o]_{j-1/2}) = -s_{o,j} Q_{p,j} / \phi \tag{5.68}$$

where

$$[s_o u_o]_{j+1/2} = \begin{cases} s_{o,j} u_{o,j+1/2}, & \text{if } u_{o,j+1/2} \geq 0; \\ s_{o,j+1} u_{o,j+1/2}, & \text{if } u_{o,j+1/2} < 0. \end{cases} \tag{5.69}$$

Step 2: Computation of velocities and pressure

Next, we solve for $P_{w,j}(t)$ and $u_{w,j+1/2}(t)$, $u_{o,j+1/2}(t)$ and $u_{g,j+1/2}(t)$ by considering the following ODE system:

$$\frac{1}{\Delta x} ([s_w u_w]_{j+1/2} - [s_w u_w]_{j-1/2}) + \frac{1}{\Delta x} ([s_o u_o]_{j+1/2} - [s_o u_o]_{j-1/2}) + \frac{1}{\Delta x} ([s_g u_g]_{j+1/2} - [s_g u_g]_{j-1/2}) = Q_{Iw,j} / \phi + Q_{Ig,j} / \phi - Q_{p,j} / \phi \tag{5.70}$$

which is combined with the momentum balance equations

$$\begin{aligned}
 s_{w,j+1/2} \frac{1}{\Delta x} (P_{w,j+1} - P_{w,j}) &= -\hat{k}_{w,j+1/2} u_{w,j+1/2} - \hat{k}_{wo,j+1/2} (u_{w,j+1/2} - u_{o,j+1/2}) - \hat{k}_{wg,j+1/2} (u_{w,j+1/2} - u_{g,j+1/2}) \\
 &\quad - g s_{w,j+1/2} \rho_w + \epsilon_w \frac{\rho_w}{\Delta x^2} (s_{w,j+1} [u_{w,j+3/2} - u_{w,j+1/2}] - s_{w,j} [u_{w,j+1/2} - u_{w,j-1/2}]), \\
 s_{o,j+1/2} \frac{1}{\Delta x} (P_{w,j+1} - P_{w,j}) &= -s_{o,j+1/2} \frac{1}{\Delta x} (\Delta P_{ow,j+1} - \Delta P_{ow,j}) \\
 &\quad - \hat{k}_{o,j+1/2} u_{o,j+1/2} - \hat{k}_{wo,j+1/2} (u_{o,j+1/2} - u_{w,j+1/2}) - \hat{k}_{og,j+1/2} (u_{o,j+1/2} - u_{g,j+1/2}) \\
 &\quad - g s_{o,j+1/2} \rho_o + \epsilon_o \frac{\rho_o}{\Delta x^2} (s_{o,j+1} [u_{o,j+3/2} - u_{o,j+1/2}] - s_{o,j} [u_{o,j+1/2} - u_{o,j-1/2}]), \\
 s_{g,j+1/2} \frac{1}{\Delta x} (P_{w,j+1} - P_{w,j}) &= -s_{g,j+1/2} \frac{1}{\Delta x} (\Delta P_{ow,j+1} - \Delta P_{ow,j} + \Delta P_{go,j+1} - \Delta P_{go,j}) \\
 &\quad - \hat{k}_{g,j+1/2} u_{g,j+1/2} - \hat{k}_{wg,j+1/2} (u_{g,j+1/2} - u_{w,j+1/2}) - \hat{k}_{og,j+1/2} (u_{g,j+1/2} - u_{o,j+1/2}) \\
 &\quad - g s_{g,j+1/2} \rho_g + \epsilon_g \frac{\rho_g}{\Delta x^2} (s_{g,j+1} [u_{g,j+3/2} - u_{g,j+1/2}] - s_{g,j} [u_{g,j+1/2} - u_{g,j-1/2}]).
 \end{aligned} \tag{5.71}$$

Here we note that the average $s_{w,j+1/2}$ in (5.71) is based on upwind relatively $u_{w,j+1/2}$

$$s_{w,j+1/2} = \begin{cases} s_{w,j}, & \text{if } u_{w,j+1/2} > 0; \\ \frac{s_{w,j} + s_{w,j+1}}{2}, & \text{if } u_{w,j+1/2} = 0; \\ s_{w,j+1}, & \text{if } u_{w,j+1/2} < 0. \end{cases} \tag{5.72}$$

Similarly, for $s_{o,j+1/2}$, $s_{g,j+1/2}$ and for the interaction terms $\hat{k}_{w,j+1/2}$, $\hat{k}_{o,j+1/2}$, and $\hat{k}_{g,j+1/2}$.

In addition, $\hat{k}_{wo,j+1/2}$ is based on upwind relatively $u_{w,j+1/2}$ and $u_{o,j+1/2}$

$$\hat{k}_{wo,j+1/2} = \begin{cases} \hat{k}_{wo,j}, & \text{if } u_{w,j+1/2} > 0 \& u_{o,j+1/2} > 0; \\ \frac{\hat{k}_{wo,j} + \hat{k}_{wo,j+1}}{2}, & \text{if } u_{w,j+1/2} u_{o,j+1/2} \leq 0; \\ \hat{k}_{wo,j+1}, & \text{if } u_{w,j+1/2} < 0 \& u_{o,j+1/2} < 0. \end{cases} \tag{5.73}$$

$\hat{k}_{wg,j+1/2}$ and $\hat{k}_{og,j+1/2}$ are also approximated using the similar way. On the other hand, $[s_w u_w]_{j+1/2}$, $[s_o u_o]_{j+1/2}$ and $[s_g u_g]_{j+1/2}$ appearing in (5.70) employ upwind as described in (5.72).

C2. A fully discrete scheme for the incompressible model

Step 1: Mass transport

$$\frac{s_{w,j}^{k+1} - s_{w,j}^k}{\Delta t} + \frac{1}{\Delta x} ([s_w u_w]_{j+1/2}^k - [s_w u_w]_{j-1/2}^k) = -s_{w,j}^k Q_{p,j}^k / \phi + Q_{Iw,j}^k / \phi \tag{5.74}$$

where

$$[s_w u_w]_{j+1/2}^k = \begin{cases} s_{w,j}^k u_{w,j+1/2}^k, & \text{if } u_{w,j+1/2}^k \geq 0; \\ s_{w,j+1}^k u_{w,j+1/2}^k, & \text{if } u_{w,j+1/2}^k < 0. \end{cases} \tag{5.75}$$

$$\frac{s_{o,j}^{k+1} - s_{o,j}^k}{\Delta t} + \frac{1}{\Delta x} ([s_o u_o]_{j+1/2}^k - [s_o u_o]_{j-1/2}^k) = -s_{o,j}^k Q_{p,j}^k / \phi \tag{5.76}$$

where

$$[s_o u_o]_{j+1/2}^k = \begin{cases} s_{o,j}^k u_{o,j+1/2}^k, & \text{if } u_{o,j+1/2}^k \geq 0; \\ s_{o,j+1}^k u_{o,j+1/2}^k, & \text{if } u_{o,j+1/2}^k < 0. \end{cases} \tag{5.77}$$

Having computed $s_{w,j}^{k+1}$ and $s_{o,j}^{k+1}$ we can compute pressure and velocities simultaneously at time level $k + 1$.

Step 2: Computation of velocities and pressure

We solve for $P_{w,j}^{k+1}$ and $u_{w,j+1/2}^{k+1}$, $u_{o,j+1/2}^{k+1}$ and $u_{g,j+1/2}^{k+1}$ by considering the following algebraic system

$$\frac{1}{\Delta x} ([s_w^{k+1} u_w^{k+1}]_{j+1/2} - [s_w^{k+1} u_w^{k+1}]_{j-1/2}) + \frac{1}{\Delta x} ([s_o^{k+1} u_o^{k+1}]_{j+1/2} - [s_o^{k+1} u_o^{k+1}]_{j-1/2}) + \frac{1}{\Delta x} ([s_g^{k+1} u_g^{k+1}]_{j+1/2} - [s_g^{k+1} u_g^{k+1}]_{j-1/2}) = Q_{I,j}^k / \phi - Q_{p,j}^k / \phi \tag{5.78}$$

which is combined with the momentum balance equations

$$\begin{aligned} s_{w,j+1/2}^{k+1/2} \frac{1}{\Delta x} (P_{w,j+1}^{k+1} - P_{w,j}^{k+1}) &= -\hat{k}_{w,j+1/2}^{k+1/2} u_{w,j+1/2}^{k+1} - \hat{k}_{wo,j+1/2}^{k+1/2} (u_{w,j+1/2}^{k+1/2} - u_{o,j+1/2}^{k+1/2}) - \hat{k}_{wg,j+1/2}^{k+1/2} (u_{w,j+1/2}^{k+1/2} - u_{g,j+1/2}^{k+1/2}) \\ &\quad - s_{w,j+1/2}^{k+1} \rho_w g + \varepsilon_w \frac{\rho_w}{\Delta x^2} (s_{w,j+1}^{k+1} [u_{w,j+3/2}^{k+1} - u_{w,j+1/2}^{k+1}] - s_{w,j}^{k+1} [u_{w,j+1/2}^{k+1} - u_{w,j-1/2}^{k+1}]) \\ s_{o,j+1/2}^{k+1/2} \frac{1}{\Delta x} (P_{w,j+1}^{k+1} - P_{w,j}^{k+1}) &= -s_{o,j+1/2}^{k+1/2} \frac{1}{\Delta x} (\Delta P_{ow,j+1}^{k+1/2} - \Delta P_{ow,j}^{k+1/2}) \\ &\quad - \hat{k}_{o,j+1/2}^{k+1/2} u_{o,j+1/2}^{k+1} - \hat{k}_{wo,j+1/2}^{k+1/2} (u_{o,j+1/2}^{k+1} - u_{w,j+1/2}^{k+1}) - \hat{k}_{og,j+1/2}^{k+1/2} (u_{o,j+1/2}^{k+1} - u_{g,j+1/2}^{k+1}) \\ &\quad - s_{o,j+1/2}^{k+1} \rho_o g + \varepsilon_o \frac{\rho_o}{\Delta x^2} (s_{o,j+1}^{k+1} [u_{o,j+3/2}^{k+1} - u_{o,j+1/2}^{k+1}] - s_{o,j}^{k+1} [u_{o,j+1/2}^{k+1} - u_{o,j-1/2}^{k+1}]) \\ s_{g,j+1/2}^{k+1/2} \frac{1}{\Delta x} (P_{w,j+1}^{k+1} - P_{w,j}^{k+1}) &= -s_{g,j+1/2}^{k+1/2} \frac{1}{\Delta x} (\Delta P_{ow,j+1}^{k+1/2} - \Delta P_{ow,j}^{k+1/2} + \Delta P_{go,j+1}^{k+1/2} - \Delta P_{go,j}^{k+1/2}) \\ &\quad - \hat{k}_{g,j+1/2}^{k+1/2} u_{g,j+1/2}^{k+1} - \hat{k}_{wg,j+1/2}^{k+1/2} (u_{g,j+1/2}^{k+1} - u_{w,j+1/2}^{k+1}) - \hat{k}_{og,j+1/2}^{k+1/2} (u_{g,j+1/2}^{k+1} - u_{o,j+1/2}^{k+1}) \\ &\quad - s_{g,j+1/2}^{k+1} \rho_g g + \varepsilon_g \frac{\rho_g}{\Delta x^2} (s_{g,j+1}^{k+1} [u_{g,j+3/2}^{k+1} - u_{g,j+1/2}^{k+1}] - s_{g,j}^{k+1} [u_{g,j+1/2}^{k+1} - u_{g,j-1/2}^{k+1}]) \end{aligned} \tag{5.79}$$

Remark 5.5. The upwind discretization of $[s_w^{k+1} u_w^{k+1}]_{j+1/2}$, $[s_o^{k+1} u_o^{k+1}]_{j+1/2}$ and $[s_g^{k+1} u_g^{k+1}]_{j+1/2}$ appearing in (5.78) are based on "old" velocities $u_{w,j+1/2}^k$, $u_{o,j+1/2}^k$ and $u_{g,j+1/2}^k$.

Appendix D. The convergence of numerical scheme

Here we illustrate one example to show the convergence of the presented numerical scheme in Appendix C for the incompressible three-phase flow. A sensitivity test is conducted by using different number of grid cells to compare the water saturation profiles for the same case as shown in Fig. 6, panel F. We refer to Fig. 11 for an illustration of the convergence test.

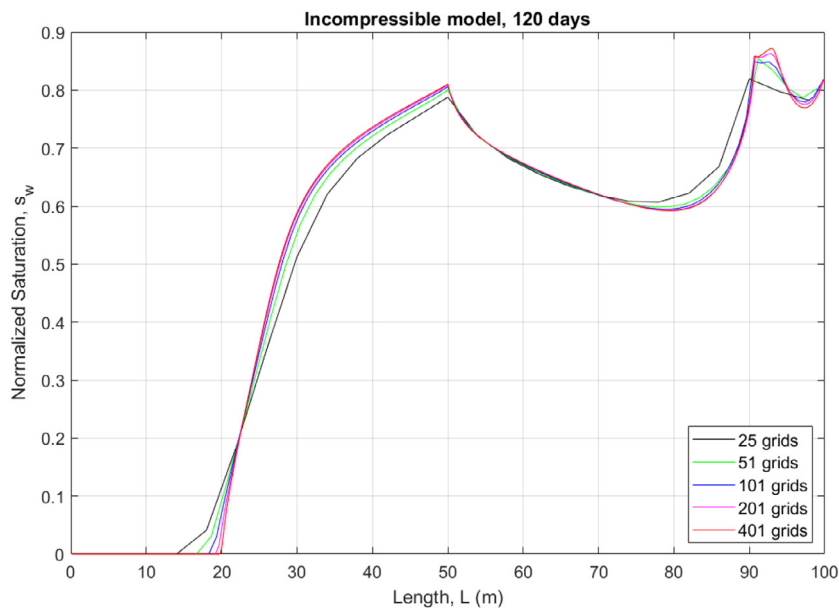


Fig. 11. Water saturation s_w profiles using different number of grid cells in the model for the case as shown in Fig. 6, panel F.

CRediT authorship contribution statement

Yangyang Qiao: Methodology, Writing - review & editing. **Steinar Evje:** Methodology, Writing - original draft.

References

- Ambrosi, D., Preziosi, L., 2002. On the closure of mass balance models for tumor growth. *Math. Models Methods Appl. Sci.* 12 (5), 737–754.
- Andersen, P.O., Qiao, Y., Standnes, D.C., Evje, S., 2019. Co-current spontaneous imbibition in porous media with the dynamics of viscous coupling and capillary back pressure. *SPE J.* 24 (1), 158–177.
- Avraam, D.G., Payatakes, A.C., 1995. Flow regimes and relative permeabilities during steady-state two-phase flow in porous media. *J. Fluid Mech.* 293, 207–236.
- Ayodele, O.R., 2006. Theoretical analysis of viscous coupling in two-phase flow through porous media. *Transp. Porous Media* 64 (2), 171–184.
- Bacri, J.C., Chaouche, M., Salin, D., 1990. Modele simple de permeabilities croisees. In: *Series II*, 311. C.R. Acad. Sci., pp. 591–596.
- Bakhshian, S., Hosseini, S.A., 2019. Pore-scale analysis of supercritical CO₂-brine immiscible displacement under fractional-wettability conditions. *Adv. Water Resour.* 126, 96–107.
- Bakhshian, S., Hosseini, S.A., Shokri, N., 2019. Pore-scale characteristics of multiphase flow in heterogeneous porous media using the lattice Boltzmann method. *Sci. Rep.* 9 (1), 1–13.
- Bentsen, R.G., Manai, A.A., 1992. Measurement of concurrent and countercurrent relative permeability curves using the steady-state method. *AOSTRA J. Res.* 7, 169–181.
- Bentsen, R.G., Manai, A.A., 1993. On the use of conventional cocurrent and countercurrent effective permeabilities to estimate the four generalized permeability coefficients which arise in coupled, two-phase flow. *Transp. Porous Media* 11, 243–262.
- Bentsen, R.G., Trivedi, J.J., 2012. Modified transport equations for the three-phase flow of immiscible, incompressible fluids through water-wet porous media. *J. Porous Media* 15 (2).
- Bourbiaux, B.J., Kalaydjian, F.J., 1990. Experimental study of cocurrent and countercurrent flows in natural porous media. *SPE Reservoir Eng.* 5 (3), 361–368.
- Bowen, R.M., 1976. *Theory of Mixtures*. In: Eringen, A.C. (Ed.), *Continuum Physics*. Academic, New York.
- Byrne, H.M., Preziosi, L., 2003. Modelling solid tumour growth using the theory of mixtures. *Math. Med. Biol.* 20 (4), 341–366.
- Chen, Z.X., Ewing, R.E., 1997. Comparison of various formulations of three-phase flow in porous media. *J. Comput. Phys.* 132, 362–373.
- de la Cruz, V., Spanos, T.J.T., 1983. Mobilization of oil ganglia. *AlChE J.* 29 (5), 854–858.
- Darcy, H., 1856. *Les Fontaines Publiques de la Ville de Dijon*. Dalmont, Paris.
- Dong, J., Riviere, B., 2016. A semi-implicit method for incompressible three-phase flow in porous media. *Comput. Geosci.* 20, 1169–1184.
- Drew, D.A., Segel, L.A., 1971. Averaged equations for two-phase flows. *Stud. Appl. Math.* 50, 205–231.
- Dullien, F.A.L., Dong, M., 1996. Experimental determination of the flow transport coefficients in the coupled equations of two-phase flow in porous media. *Transp. Porous Media* 25, 97–120.
- Ehrlich, R., 1993. Viscous coupling in two-phase flow in porous media and its effect on relative permeabilities. *Transp. Porous Media* 11 (3), 201–218.
- Evje, S., 2017. An integrative multiphase model for cancer cell migration under influence of physical cues from the tumor microenvironment. *Chem. Eng. Sci.* 165, 240–259.
- Evje, S., Waldeland, J.O., 2019. How tumor cells can make use of interstitial fluid flow in a strategy for metastasis. *Cel. Mol. Bioeng.* 12, 227–254.
- Falls, A.H., Schulte, W.M., 1992. Theory of three component, three phase displacement in porous media. *SPE Reserv. Eng.* 7 (3), 377–384.
- Gajo, A., Cecinato, F., Lore, B., 2017. Deformable porous media saturated by three immiscible fluids: constitutive modelling and simulations of injection and imbibition tests. *Transp. Porous Media* 116, 19–51.
- Guzmán, R.E., Fayers, F.J., 1997. Mathematical properties of three-phase flow equations. *Soc. Pet. Eng. J.* 2 (3), 291–300.
- Guzmán, R.E., Fayers, F.J., 1997. Solution to the three-phase buckley–leverett problem. *Soc. Pet. Eng. J.* 2 (3), 301–311.
- Juanes, R., 2008. Nonequilibrium effects in models of three-phase flow in porous media. *Adv. Wat. Res.* 31, 661–673.
- Juanes, R., Patzek, T.W., 2004. Analytical solution to the riemann problem of three-phase flow in porous media. *Transp. Porous Media* 55 (1), 47–70.
- Kalaydjian, F., 1987. A macroscopic description of multiphase flow in porous media involving spacetime evolution of fluid/fluid interface. *Transp. Porous Media* 2, 537–552.
- Kalaydjian, F., 1990. Origin and quantification of coupling between relative permeabilities for two-phase flows in porous media. *Transp. Porous Media* 5 (3), 215–229.
- Katchalsky, A., Curran, P.A., 1975. *Nonequilibrium Thermodynamics in Biophysics*. Harvard University Press, Cambridge.
- Labernadie, A., et al., 2017. A mechanically active heterotypic E-cadherin/N-cadherin adhesion enables fibroblasts to drive cancer cell invasion. *Nat. Cell. Biol.* 19, 224–236.
- Langaas, K., Papatzacos, P., 2001. Numerical investigations of the steady state relative permeability of a simplified porous medium. *Transp. Porous Media* 45, 241–266.
- Lee, S.H., Efeendiev, Y., 2016. c¹-continuous relative permeability and hybrid upwind discretization of three phase flow in porous media. *Adv. Water Resour.* 96, 209–224.
- Lee, S.H., Wolfsteiner, C., Tchelepi, H.A., 2008. Multiscale finite-volume formulation for multiphase flow in porous media: black oil formulation of compressible, three-phase flow with gravity. *Comput. Geosci.* 12, 351–366.
- Lewis, R., Pao, W., 2002. Numerical simulation of three-phase flow in fractured reservoirs. *Gas Sci. Technol. - Revue d'IFP Energies nouvelles* 57, 499–514.
- Li, H., Pan, C., Miller, C.T., 2004. Viscous coupling effects for two-phase flow in porous media. *Dev. Water Sci.* 55 (Part 1), 247–256.
- Li, H., Pan, C., Miller, C.T., 2005. Pore-scale investigation of viscous coupling effects for two-phase flow in porous media. *Phys. Rev. E* 72.
- Lie, K.A., Juanes, R., 2005. A front-tracking method for the simulation of three-phase flow in porous media. *Comput. Geosci.* 9, 29–59.
- Muskat, M., Wyckoff, R.D., Botset, H.G., Meres, M.M., 1937. Flow of gas-liquid mixtures through sands. *SPE Trans. AIME* 123 (1), 69–96.
- Odd, S.H., David, J.B., 2010. A fully coupled three-phase model for capillary pressure and relative permeability for implicit compositional reservoir simulation. *SPE J.* 15 (SPE-125429-PA).
- Polacheck, W.J., Charest, J.L., Kamm, R.F., 2011. Interstitial flow influences direction of tumor cell migration through competing mechanisms. *PNAS* 108, 11115–11120.
- Preziosi, L., Farina, A., 2002. On darcy's law for growing porous media. *Int. J. Non Linear Mech.* 37, 485–491.
- Qiao, Y., Andersen, P.O., Evje, S., Standnes, D.C., 2018. A mixture theory approach to model co- and counter-current two-phase flow in porous media accounting for viscous coupling. *Adv. Water Resour.* 112, 170–188.
- Qiao, Y., Wen, H., Evje, S., 2019. Compressible and viscous two-phase flow in porous media based on mixture theory formulation. *Netw. Heterogen. Media* 14, 489–536.

- Qiao, Y., Wen, H., Evje, S., 2019. Viscous two-phase flow in porous media driven by source terms: analysis and numerics. *SIAM J. Math. Anal.* 51, 5103–5140.
- Rajagopal, K.R., 2007. On a hierarchy of approximate models for flows of incompressible fluids through porous solids. *Math. Mod. Met. Appl. Sci.* 17, 215–252.
- Rajagopal, K.R., Tao, L., 1995. *Mechanics of Mixtures*. Series on Advances in Mathematics for Applied Sciences- Vol. 35. World Scientific.
- Ranaee, E., Inzoli, F., Riva, M., Guadagnini, A., 2019. Hysteresis effects of three-phase relative permeabilities on black-oil reservoir simulation under WAG injection protocols. *J. Petrol. Sci. Eng.* 176, 1161–1174.
- Rose, W., 2000. Myths about later-day extensions of Darcy's law. *J. Petroleum Sci. Eng.* 26, 187–198.
- Sherafati, M., Jessen, K., 2017. Dynamic relative permeability and simulation of WAG injection processes. *Transp. Porous Media* 117, 125–147.
- Shieh, A.C., Rozansky, H.A., Hinz, B., Swartz, M.A., 2011. Tumor cell invasion is promoted by interstitial flow-induced matrix priming by stromal fibroblasts. *Cancer Res.* 71, 790–800.
- Standnes, D.C., Evje, S., Andersen, P.O., 2017. A novel relative permeability model based on mixture theory approach accounting for solid–fluid and fluid–fluid interactions. *Transp. Porous Media* 119, 707–738.
- Urdal, J., Waldeland, J.O., Evje, S., 2019. Enhanced cancer cell invasion caused by fibroblasts when fluid flow is present. *Biomech. Model. Mechanobiol.* 18, 1047–1078.
- Waldeland, J.O., Evje, S., 2018. Competing tumor cell migration mechanisms caused by interstitial fluid flow. *J. Biomech.* 81, 22–35.
- Waldeland, J.O., Evje, S., 2018. A multiphase model for exploring cancer cell migration driven by autologous chemotaxis. *Chem. Eng. Sci.* 119, 268–287.
- Wu, Y.S., 2016. *Multiphase Fluid Flow in Porous and Fractured Reservoirs*. Elsevier.
- Yuster, S.T., 1951. Theoretical considerations of multiphase flow in idealized capillary systems. In: *World Petroleum Cong. Proc., Section II, The Hague*, pp. 437–445.